



## Magnetoelastic coupling behaviour of nanocrystalline $\epsilon$ -Fe<sub>2</sub>O<sub>3</sub>

C.R.S. Haines<sup>a</sup>, M. Gich<sup>b</sup>, J.L. García-Muñoz<sup>b</sup>, A. Romaguera<sup>b</sup>, Z. Ma<sup>b</sup>, M.B. Costa<sup>c</sup>, M. A. Carpenter<sup>a,\*</sup>

<sup>a</sup> Department of Earth Sciences, University of Cambridge, Downing Street, Cambridge CB2 3EQ, United Kingdom

<sup>b</sup> Institut de Ciència de Materials de Barcelona (ICMAB-CSIC), Campus UAB, 08193 Bellaterra, Spain

<sup>c</sup> Department of Materials Science and Metallurgy, University of Cambridge, 27 Charles Babbage Road, Cambridge CB3 0FS, United Kingdom

### ARTICLE INFO

#### Keywords:

Magnetoelastic coupling  
Strain relaxation  
Nanocrystalline  
Magnetic phase transition  
 $\epsilon$ -Fe<sub>2</sub>O<sub>3</sub>

### ABSTRACT

Preparation of a ceramic sample which preserved the nanoscale grain sizes of  $\sim$ 10–30 nm has allowed elastic and anelastic properties of  $\epsilon$ -Fe<sub>2</sub>O<sub>3</sub> to be investigated as functions of temperature and magnetic field strength by Resonant Ultrasound Spectroscopy in the frequency range  $\sim$ 0.1–1 MHz. Formal analysis of spontaneous strains,  $e$ , from previously obtained high resolution lattice parameter data confirmed that magnetic ordering below  $\sim$ 500 K is accompanied by strains of up to  $\sim$  $\pm$ 0.002 due to coupling with the order parameter,  $m$ , according to  $\lambda em^2$ . However, this coupling does not result in elastic softening that would be expected if the order parameter relaxed in response to an induced strain on the timescale of the acoustic resonances. Stiffening or softening during heating through  $\sim$ 450–480 K of the initial as prepared material, which acquired a distinct magnetisation parallel to the stress applied during Spark Plasma Sintering, is attributed to changes in magnetic domain configurations involving preferred local alignments of individual moments of monodomain crystals. The crystallographic space group,  $Pna2_1$ , and magnetic space group at room temperature,  $Pna'2_1$ , allow  $\epsilon$ -Fe<sub>2</sub>O<sub>3</sub> to be both piezoelectric and piezomagnetic. It is postulated that changes in the effective coefficients of these properties for bulk samples are responsible for the observed variations in acoustic resonance frequencies according to the magnetic domain structure present. No elastic or anelastic anomalies were observed at the commensurate-incommensurate transition near 110 K. Instead, acoustic resonance frequencies changed in response to an applied magnetic field, consistent with viscous motion of magnetic domain walls and the effect of poling on piezo coefficients. Ceramic samples of  $\epsilon$ -Fe<sub>2</sub>O<sub>3</sub> could have potentially functional piezoelectric and/or piezomagnetic properties that are tunable by choice of magnetic and thermal history.

### 1. Introduction

$\epsilon$ -Fe<sub>2</sub>O<sub>3</sub> occurs in nature as the mineral luogufengite [1] and is the stable polymorph of Fe<sub>2</sub>O<sub>3</sub> over a wide range of temperatures and pressures when the grain size is in the range  $\sim$ 10–150 nm [2,3]. Some of the rich diversity of properties it displays is due to the presence of four distinct magnetic sublattices in a frustrated crystal structure of polar symmetry,  $Pna2_1$  [4–9]. In thin film form  $\epsilon$ -Fe<sub>2</sub>O<sub>3</sub> is both ferrimagnetic and ferroelectric, with a small magnetoelectric coupling, making it a potentially significant multiferroic material at room temperature [10]. Powder and ceramic samples are also ferrimagnetic but, although they show a degree of magnetoelectric coupling, no evidence has been found for ferroelectric switching [6,11]. Successful preparation of a ceramic sample by spark plasma sintering, without any significant increases in grain size, has allowed the bulk dielectric properties to be measured

[11]. However, until now no attempts to measure elastic properties or to investigate strain relaxation behaviour accompanying the magnetic ordering have been reported. The primary objective of the study reported here was to fill this gap, firstly by presenting a conventional analysis of strain coupling with the magnetic order parameters and, secondly, by reporting variations of elastic and anelastic properties as functions of temperature and magnetic field obtained by Resonant Ultrasound Spectroscopy (RUS).

Powder diffraction measurements have confirmed that the crystallographic structure of nanocrystalline  $\epsilon$ -Fe<sub>2</sub>O<sub>3</sub> can be refined in space group  $Pna2_1$  between at least 10 and 923 K [5,12]. It was commonly accepted that a paramagnetic to ferrimagnetic transition occurred with falling temperature at  $\sim$ 500 K [7,8,12]. However, Garcia-Muñoz et al [12] proposed that an ordered, weakly ferrimagnetic structure persists up to a higher transition temperature ( $\sim$ 850 K). Upon cooling from the

\* Corresponding author.

E-mail address: [mc43@esc.cam.ac.uk](mailto:mc43@esc.cam.ac.uk) (M.A. Carpenter).

<https://doi.org/10.1016/j.jmmm.2022.170240>

Received 23 August 2022; Received in revised form 8 November 2022; Accepted 24 November 2022

Available online 28 November 2022

0304-8853/© 2022 The Authors. Published by Elsevier B.V. This is an open access article under the CC BY license (<http://creativecommons.org/licenses/by/4.0/>).

stability field of the paramagnetic phase, a ferrimagnetic structure, named FM1, develops first between  $T_{N1}$  (~850 K) and  $T_{N2}$  (~480 K). With further cooling this is replaced by a second ferrimagnetic structure, FM2, which is stable between  $T_{N2}$  and 150 K. The two ferrimagnetic structures share the same magnetic space group  $Pna'2_1'$  [12]. FM2 exhibits a high coercivity at room temperature but this reduces steeply with falling temperature below ~150 K [13–17], in association with the development of incommensurate magnetic ordering [6,18,19]. In measuring fields of 100 and 1000 Oe, the onset of declining magnetisation with falling temperature occurs at ~150 K, the onset of the steepest reduction occurs at ~110 K and levelling off to values approaching zero occurs below ~80 K [18]. Commensurate and incommensurate magnetic ordering reflections coexist in neutron powder diffraction patterns between ~110 and ~80 K. The out-of-phase component of ac magnetic susceptibility measured at 1 kHz has a peak at 91 and 101 K [5]. There is a small excess heat capacity below ~130 K, which Gich et al [18] interpreted in terms of a second order magnetic and structural transition.

Spontaneous strains arising from coupling with the order parameter at a phase transition are typically on the order of a few per mil to a few per cent (e.g. Ref. [20]). These, in turn, give rise to elastic anomalies which may be substantially greater, i.e. on the order of 10's of per cent, and typically have patterns that are indicative both of the form and strength of the coupling [21–23]. Direct evidence for measurable spontaneous strain due to coupling with the magnetic order parameters in  $\epsilon$ -Fe<sub>2</sub>O<sub>3</sub> is provided by changes in thermal expansion at ~500 K [12] and more subtle variations in lattice parameters between ~80 and 150 K [19]. It might be expected, therefore, that there will also be variations in elastic properties and, if any aspect of the resulting transformation microstructures is coupled with strain and mobile, also in acoustic loss. However, results from RUS presented here do not show classical patterns of anomalies, with implications for the dynamics of the strain/order parameter coupling. Instead, changes in elastic properties appear to depend on variations of piezoelectric and/or piezomagnetic effects which themselves depend on magnetic domain structures arising from interaction of magnetic dipoles of monodomain grains and thermal history.

## 2. Sample description and methods

### 2.1. Sample preparation

Single crystalline  $\epsilon$ -Fe<sub>2</sub>O<sub>3</sub> nanoparticles embedded in a silica matrix were prepared using the sol–gel based method. Hydrated iron (III) nitrate Fe(NO<sub>3</sub>)<sub>3</sub>·9H<sub>2</sub>O (Aldrich) was used as the Fe precursor and tetraethyl orthosilicate (TEOS, Si(OC<sub>2</sub>H<sub>5</sub>)<sub>4</sub>) (Aldrich) was the metal alkoxide precursor for the formation of the SiO<sub>2</sub> matrix. The silica matrix plays an important role in limiting the growth of  $\epsilon$ -Fe<sub>2</sub>O<sub>3</sub> particles, preventing their transformation to  $\alpha$ -Fe<sub>2</sub>O<sub>3</sub> [24]. The iron oxide content with respect to silica was fixed to 24 wt%, while the molar ratios of TEOS, ethanol and water were 1:6:6. First, 8.61 g of iron (III) nitrate nonahydrate were dissolved in a solution of Milli-Q water (6.23 mL) and ethanol (31.42 mL) under stirring. After dissolution of the iron nitrate the pH of the solution was ~0.35. 20 mL of TEOS were then added dropwise into the solution while stirring continuously. Stirring was maintained for ~15 min after the addition of TEOS in order to obtain a stable, clear and homogeneous solution. The final sol was distributed into four Petri dishes with 9 cm diameter, which were covered, placed inside a plastic box and kept in a chemical hood for around two weeks until gelation occurred. The gels were crushed in a ceramic mortar and further air-dried at 60 °C for 24 h.

The dried xerogel was ground thoroughly and the resulting powder placed in an alumina boat for heating up to 1100 °C in air, using a heating rate of 80 °C.hr<sup>-1</sup>. The sample was held for two hours at 1100 °C before being cooled to room temperature at 350 °C.hr<sup>-1</sup>. In order to remove the silica by chemical etching, 3 g were further ground into a

fine powder and added to a concentrated NaOH aqueous solution (12 M) in a round-bottomed flask, immersed in an oil bath at 80 °C. The mixture was stirred vigorously for 48 hr while water vapor was refluxed using a water-refrigerated condenser. Products were collected by centrifuging at 6000 rpm and the supernatant was discarded. The solid was redispersed in distilled water and the centrifuging/washing cycle was repeated twice. The final precipitates were air-dried at 60 °C for 24 hr.

In order to produce a ceramic sample for RUS measurements, about 330 mg of nanoparticles were sintered into a disc of diameter 10 mm by Spark Plasma Sintering for 4 min at 350 °C under a pressure 100 MPa, making use of the Plateforme Nationale de Frittage Flash facility at Université Toulouse III-CNRS. The resulting disc was ~2.2 mm thick and had a porosity of 38 %.

The top and bottom surfaces of the sintered disc were ground down to a final thickness of ~1.5 mm. It was then cut into rectangular parallelepipeds with a fine annular saw, lubricated with paraffin. The piece used for low temperature RUS measurements (Sample #1) had dimensions 1.556x1.739x2.235 mm<sup>3</sup> and mass 18.4 mg. Several pieces, not necessarily with perfect parallelepiped shapes, were used for different combinations of RUS measurements at high temperatures: 1.533x1.714x2.241 mm<sup>3</sup>, 17.9 mg (Sample #2); 1.516x1.759x2.238 mm<sup>3</sup>, 18.4 mg (sample #3); 1.486x1.713x2.220 mm<sup>3</sup>, 15.2 mg (Sample #4); 1.558x1.715x2.239 mm<sup>3</sup>, 18.2 mg (Sample #5). A further parallelepiped (sample #6, 2.726x1.716x1.566 mm<sup>3</sup>, 21.3 mg) was used to check magnetisation in directions parallel to its principal axes before and after heating to 539 K.

A separate piece remaining from a different sintered disc which had been prepared for other measurements was also used for high temperature RUS measurements. This is referred to below as “Second Slice”. It had parallel sides and thickness 0.576 mm, with an irregular shape of ~2.5 × 2.5 mm<sup>2</sup> in the other two dimensions. The mass was 8.6 mg.

### 2.2. Sample characterisation: TEM, X-ray diffraction, differential scanning calorimetry

The powdered sample prepared for sintering was examined by transmission electron microscopy in a Jeol 1210 microscope at 120 kV. As shown in Fig. 1a, it contained approximately spherical nanoparticles with sizes slightly above 20 nm. A log-normal distribution for the sizes of more than 600 nanoparticles, measured from TEM images using the ImageJ software [25] gave a peak at ~18 nm (Fig. 1b).

X-ray diffraction patterns of nanoparticles in the powder sample and of the sintered disk were obtained using a Siemens D5000 diffractometer with Bragg-Brentano geometry and CuK $\alpha$  radiation. Refinements using the Materials Analysis Using Diffraction software (MAUD) [26] indicated that both the powder and the sintered disc consisted of  $\epsilon$ -Fe<sub>2</sub>O<sub>3</sub> nanoparticles with less than 5% of  $\alpha$ -Fe<sub>2</sub>O<sub>3</sub> as an impurity phase. No evidence was found for the presence of maghemite. The average crystallite diameter of  $\epsilon$ -Fe<sub>2</sub>O<sub>3</sub> particles obtained in both cases was 25 nm. This is in good agreement with the particle size distribution from TEM if account is taken of the fact that larger grains, from 18 nm as the probability maximum up to 30 nm for the largest grains, make a disproportionate contribution to the volume of crystals analysed by diffraction. Lattice parameters of the  $\epsilon$ -Fe<sub>2</sub>O<sub>3</sub> nanoparticles before sintering ( $a$  = 5.092(2) Å,  $b$  = 8.790(3) Å,  $c$  = 9.476(2) Å) and after sintering ( $a$  = 5.094(2) Å,  $b$  = 8.794(4) Å,  $c$  = 9.483(3) Å) were closely similar. The sintering process thus does not appear to have had a substantial effect on as-prepared  $\epsilon$ -Fe<sub>2</sub>O<sub>3</sub> nanoparticles other than binding them together into the form of a ceramic with ~40% porosity.

A similar sample prepared according to the method described above but not sintered was studied between 100 and 804 K by synchrotron X-ray diffraction. Diffraction patterns were collected at the BL04-MSPD beamline of the ALBA Synchrotron (Barcelona, Spain) using  $\lambda$  = 0.413480 Å. Above 300 K the sample was heated at a rate of 3 K.min<sup>-1</sup> using a Cyberstar-FMB Oxford hot air blower, with acquisition times of 100 s per pattern. Below 300 K the heating rate (using an Oxford

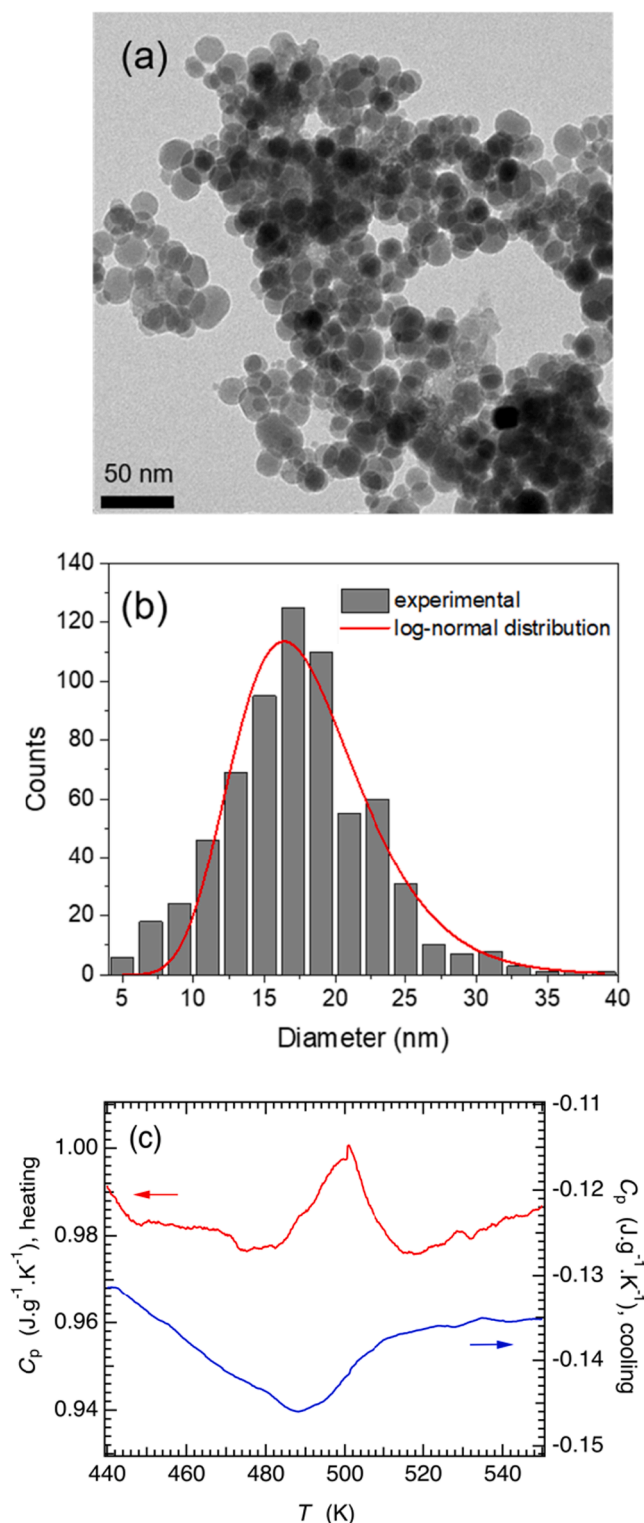


**Fig. 1.** (a) Representative TEM image of  $\epsilon$ -Fe<sub>2</sub>O<sub>3</sub> nanoparticles prior to sintering. (b) Particle size distribution from measurement of the dimensions of more than 600 grains. The red line is a log-normal distribution, with the most probable diameter at  $\sim 18$  nm. (c) Broad, weak heat capacity anomalies in the vicinity of the expected transition temperature of  $\sim 500$  K, as observed during heating (red curve, left axis) and cooling (blue curve, right axis) of an offcut from the sintered pellet at  $10 \text{ K}\cdot\text{min}^{-1}$  in a differential scanning calorimeter.

Cryostream) was  $5 \text{ K}\cdot\text{min}^{-1}$ , with acquisition time of 50 s per pattern. Lattice parameters determined from these measurements were used for the strain analysis presented below.

Heat flow was measured as a function of temperature for a 12.3 mg offcut from the sintered pellet using a TA Instruments Q2000 differential scanning calorimeter with a heating/cooling rate of  $10 \text{ K}\cdot\text{min}^{-1}$ . Fig. 1c shows small broad peaks in heat capacity centered at  $\sim 500$  K during heating and  $\sim 450$  K during cooling. Anomalies with less convincing form in relation to background noise were present in data from a second sample with mass 13.3 mg, but both are at least consistent with the expected high temperature transition occurring in the sample used for RUS.

### 2.3. Sample characterisation: Magnetism

Considering a magnetocrystalline anisotropy of  $K = 5 \times 10^5 \text{ J}\cdot\text{m}^{-3}$  and a saturation magnetization of  $M_s = 100 \text{ kA}\cdot\text{m}^{-1}$  for  $\epsilon$ -Fe<sub>2</sub>O<sub>3</sub> at room temperature [15], together with an exchange stiffness of  $A = 10^{-12} \text{ J}\cdot\text{m}^{-1}$ , obtained from  $M_s(T)$  [27] close to the FM2 to FM1 transition, an estimate of the size above which single domain  $\epsilon$ -Fe<sub>2</sub>O<sub>3</sub> particles would be no longer energetically favoured ( $D_{sd} \sim 2(AK)^{1/2}/\mu_0 M_s^2$ ) gives  $D_{sd} \sim 100$  nm [28]. Since the diameter of individual grains in the ceramic sample was in the range 5–40 nm, they must each have been a single magnetic domain.

After low temperature RUS measurements had been completed on Sample #1, the surfaces were ground away because of concern that discoloration of the surface might have been contamination. The reduced mass was 14.2 mg and a repeat cooling sequence showed that the change in sample size had not made any difference to the form of the RUS results. DC magnetic measurements were made on this reduced piece using a Quantum Design MPMS in the Maxwell Centre, University of Cambridge. Variations of magnetisation,  $M$ , measured during heating in a 50 Oe field following cooling in zero field are given in Fig. 2a. The derivative,  $dM/dT$ , is given in Fig. 2b. These show the pattern that is typical of  $\epsilon$ -Fe<sub>2</sub>O<sub>3</sub> nanoparticles [13,14,16,17]. In the present case, the first break in slope occurs at 144 K, the second at 110 K (Fig. 2b), and  $dM/dT$  levels off at  $\sim 50$  K. Gich [15] showed a double peak at  $\sim 90$  K and 101 K, but a different particle size distribution is likely to be the cause.

Hysteresis ( $M-H$ ) loops were collected from the same piece at 5, 70, 140, 200 and 300 K, and are shown together with the derivatives  $dM/dH$  in Fig. 2c and 2d, respectively. The pattern of open loops is closely similar to data in the literature from powdered samples and from dispersed particles of  $\epsilon$ -Fe<sub>2</sub>O<sub>3</sub>, with a signature drop in values of coercivity below  $\sim 150$  K (e.g. [12–15,17,19]). A maximum value of  $M = 16.4 \text{ emu}\cdot\text{g}^{-1}$  was obtained at 7 T, 5 K ( $0.24 \mu_B$  per Fe atom). The magnetization at high field and the coercivity values measured for the sintered disk are in reasonable agreement with those given by Gich [15] for particles with average grain size  $\sim 20$ –25 nm dispersed in a silica matrix.

In order to test for bulk magnetic anisotropy of the ceramic,  $M-H$  data were collected at room temperature in directions parallel to each of the principal axes of Sample #6, firstly in its virgin state, i.e. as pressed and sintered, and then following heat treatment to 539 K in the high T RUS instrument. Fig. 3a shows the measured magnetisation from data collected in the sequence  $0 \rightarrow 50 \rightarrow -50 \rightarrow 0$  Oe, and clearly reveals a marked anisotropy. Magnetisation parallel to the short direction of the parallelepiped was  $\sim 0.5 \text{ emu}\cdot\text{g}^{-1}$  and  $\sim 0$  in the other two directions. In contrast, no measurable magnetisation was detected in zero field for any direction after the heat treatment. For all samples the short edge was parallel to the direction of stress applied during Spark Plasma Sintering and the other two directions were in the plane of the original pellet, i.e. perpendicular to the applied stress.

The coercivity of  $\epsilon$ -Fe<sub>2</sub>O<sub>3</sub> is sufficiently small below  $\sim 100$  K for a 50 Oe field to reorient the direction of magnetisation. As a consequence, measurement of magnetisation during heating in a 50 Oe field, following cooling in zero field, produced closely similar magnetisation curves in

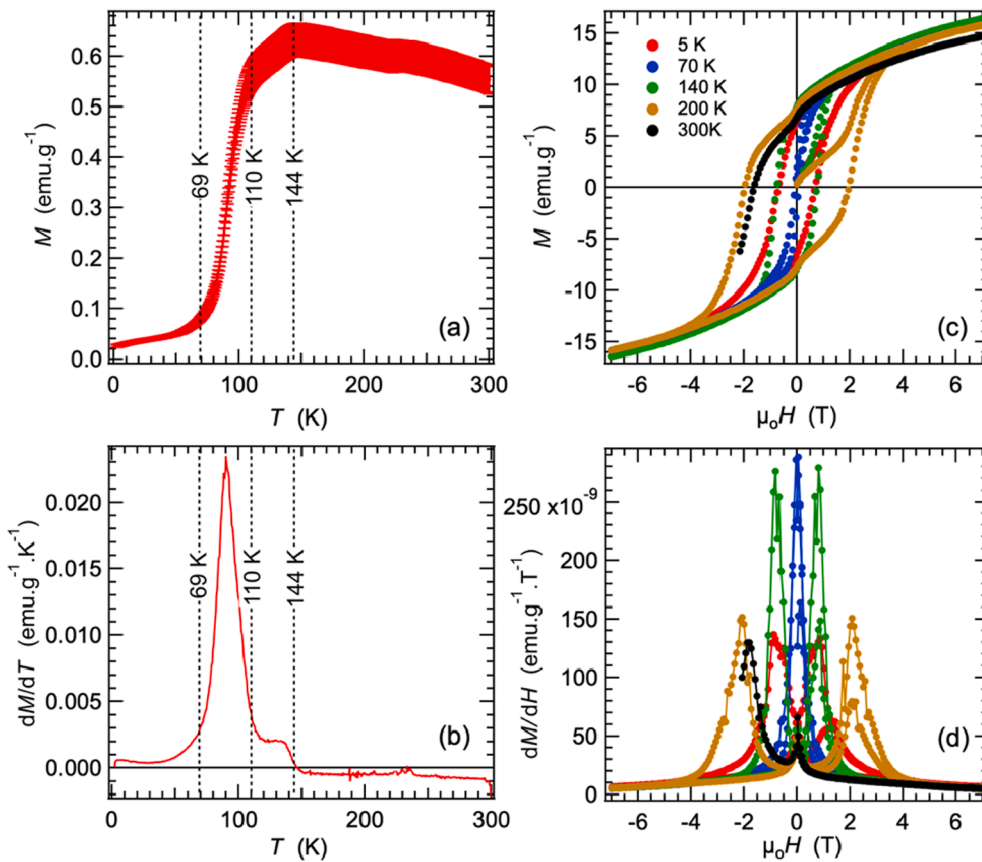


Fig. 2. Magnetic data for a 14.2 mg piece of the pellet of  $\epsilon$ - $\text{Fe}_2\text{O}_3$  used for RUS measurements at low temperatures. (a) Magnetisation,  $M$ , measured during heating in a field of 50 Oe, following cooling in zero field. The anomaly at  $\sim 230$  K is believed to be an artefact or due to the Morin transition in the small proportion of  $\alpha$ - $\text{Fe}_2\text{O}_3$  present in the sample. (b) Derivative of magnetisation with respect to temperature. (c) Hysteresis loop at different temperatures. (The 300 K loop was not finished). (d)  $dM/dH$  from the data shown in (c).

each of the three principal directions of the parallelepipeds, irrespective of whether they were in their initial state (Sample #4, Fig. 3b) or after heating to  $\sim 520$  K (Sample #5, Fig. 3c). These data reveal small differences in magnetisation above  $\sim 100$  K, such that the highest values were for measurements parallel to the long direction and lowest parallel to the short direction. If the orientation of grains and the distribution of pore spaces within the ceramic had been random, these values would be expected to be the same, irrespective of measuring direction. Thus the bulk samples were characterised by a degree of magnetic anisotropy which disappeared on heating to  $\sim 520$ – $540$  K and a degree of anisotropy with respect to average crystallographic orientation or density which did not.

Evidence for the presence of  $\alpha$ - $\text{Fe}_2\text{O}_3$  grains with dimensions greater than 100 nm would be provided by a distinct anomaly in the temperature dependence of magnetisation at 250–260 K due to the Morin transition. The transition temperature reduces with decreasing grain size and disappears entirely when the grain size reduces below 20 nm [29]. On this basis, the weak feature at  $\sim 230$  K in Fig. 2a and 3c might be attributable to the Morin transition in the small component of  $\alpha$ - $\text{Fe}_2\text{O}_3$  known to be present.  $\epsilon$ - $\text{Fe}_2\text{O}_3$  crystals in powder form do not transform to  $\alpha$ - $\text{Fe}_2\text{O}_3$  during heating up to at least 923 K [12], but stability against transformation has not been tested for a ceramic. Given that the anomaly near 230 K in Fig. 3c is no greater than that in Fig. 2a, it is assumed that significant transformation did not occur in samples heated to at least 520 K.

#### 2.4. Resonant Ultrasound Spectroscopy

RUS spectra were collected at low temperatures with and without applied magnetic field in an Oxford Instruments Teslatron cryostat described in detail elsewhere [30,31]. Sample #1 was held lightly across a pair of faces directly between the piezoelectric transducers in the

sample holder described by McKnight et al [32]. Spectra were collected in automated heating and cooling cycles at zero or constant magnetic field, or as functions of field at constant temperature. A settle time of 20 min was included before the start of data collection at each temperature to allow for thermal equilibration. The settle time before data collection when varying the magnetic field strength at constant temperature was 5 min.

For high temperature measurements, each of three rectangular parallelepipeds (Samples #2, #3, #5) was held lightly across a pair of corners between the tips of alumina buffer rods which were inserted into a horizontal tube furnace [33,34]. The Second Slice was held across opposite edges. Temperature was recorded from a thermocouple placed within a few mm of the sample, including a final calibration based on the transition temperatures of standard samples. Spectra were collected in automated heating and cooling cycles with a settle time of 20 min before data collection at each set point.

Analysis of RUS data was initiated by fitting individual resonance peaks in the primary spectra with an asymmetric Lorentzian function to obtain values of the peak frequency,  $f$ , and width at half maximum height,  $\Delta f$ . Elastic moduli of the sample scale with  $f^2$  and acoustic loss is expressed in terms of the inverse mechanical quality factor,  $Q^{-1}$ , which is taken to be  $\Delta f/f$ . Most resonances of a small sample are dominated as shearing motion so that, as here, variations of  $f^2$  reflect variations of the shear modulus. Acoustic loss is due to the motion of some part of the sample in response to shear stress on the time scale of the resonance modes, i.e.  $\sim 10^{-5}$ – $10^{-6}$  s for resonances in the frequency range  $\sim 100$  kHz–1 MHz.

Attempts to determine absolute values of elastic moduli for the rectangular parallelepipeds at room temperature were made by fitting to the frequencies of up to 20 resonance peaks in the interval  $\sim 400$ – $1200$  kHz using the software described by Migliori et al [35]. For an isotropic material there are two independent moduli, the bulk modulus ( $K$ ) and

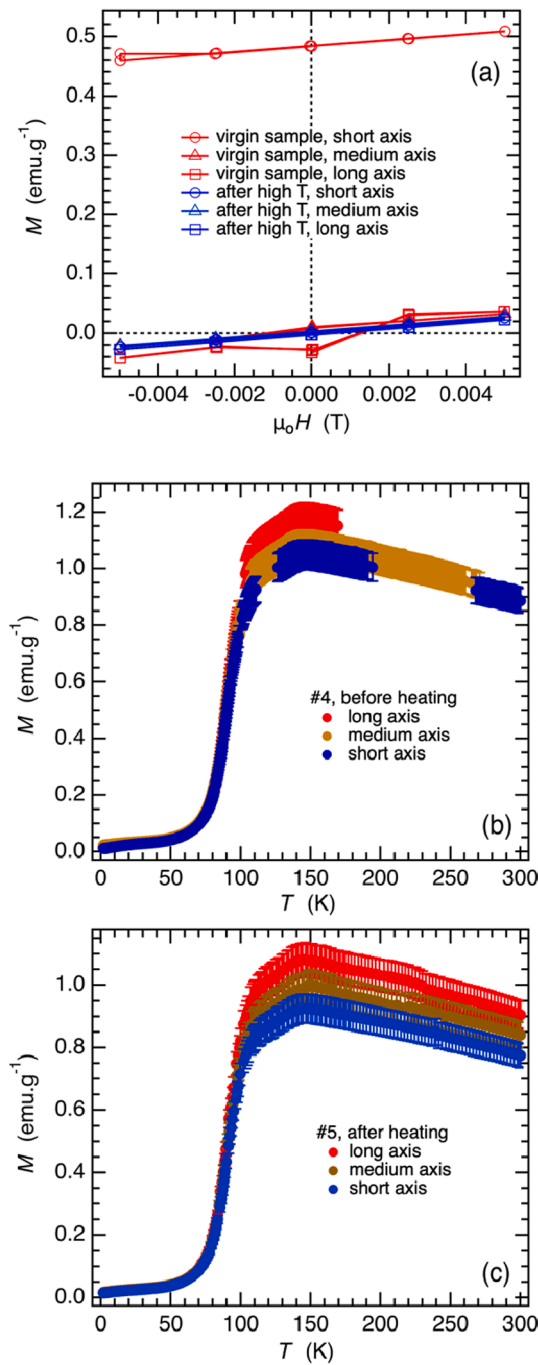


**Fig. 3.** Anisotropy of bulk samples. Error bars were taken directly from the QD MultiVu software and do not signify that the data are intrinsically noisy. (a)  $M$ - $H$  curves measured at 300 K over a limited range of small fields show significant magnetisation parallel to the short edge of Sample #5 in its virgin (as sintered) state (red) but none in any direction of the same sample following heat treatment to  $\sim 540$  K. (b), (c) Magnetisation determined during heating in a 50 Oe field, following cooling in zero field, reveal a slight anisotropy with respect to measuring direction for both a virgin sample (Sample #4) and a sample heat treated to  $\sim 520$  K (Sample #5). (Gaps in the data for Sample #4 were due to an instrument fault). It should be noted that the 50 Oe measuring field is sufficient to change the magnetisation of  $\epsilon$ -Fe<sub>2</sub>O<sub>3</sub> at low temperatures and that this would account for the differences between (a) and (b), even though the data in (b) were collected from a sample in its nominally virgin state.

the shear modulus ( $G$ ). Attempts to achieve fits were also made with five (transversely isotropic) and nine (orthotropic) independent moduli.

### 3. Strain analysis

The most direct evidence of coupling between strain and the driving order parameter for a phase transition can be obtained by analysing variations of lattice parameters. As observed at the magnetic ordering transition with  $T_N \approx 950$  K in hematite [36,37], the magnetic transition in  $\epsilon$ -Fe<sub>2</sub>O<sub>3</sub> is accompanied by overt anomalies in the temperature dependence of lattice parameters below  $\sim 500$  K [12]. There is no change in crystal system at this transition so there are three linear strains, given by  $e_1 = (a - a_0)/a_0$ ,  $e_2 = (b - b_0)/b_0$ ,  $e_3 = (c - c_0)/c_0$ , where  $a_0$ ,  $b_0$ ,  $c_0$ , are values of the high temperature structure extrapolated into the stability field of the low temperature structure. The volume strain is given by  $V_s = (V - V_0)/V_0$  which is equivalent, to good approximation, to  $e_1 + e_2 + e_3$ .

Fig. 4 shows a set of lattice parameter data in the temperature interval 100–803 K, obtained by refinement of the synchrotron X-ray diffraction data from a powdered sample of  $\epsilon$ -Fe<sub>2</sub>O<sub>3</sub> with an average grain size of 25 nm. Solid curves are fits of the function  $a_0 = a_1 + a_2 \Theta_s \coth(\Theta_s/T)$ , and similarly for  $b_0$ ,  $c_0$ ,  $V_0$ , where  $a_1$  and  $a_2$  are fit coefficients,  $T$  is temperature and  $\Theta_s$  is a saturation temperature that results in zero slope as  $T \rightarrow 0$  K [38–42].  $\Theta_s$  was set at 300 K to give flattening of the curves below  $\sim 150$  K. Values of the parameters  $a_1$ ,  $a_2$ , were obtained by fitting to data in the interval 598–803 K.

This conventional analysis of spontaneous strains associated specifically with changes in structure near 500 K gives the variations of  $e_1$ ,  $e_2$ ,  $e_3$  and  $V_s$  shown in Fig. 5. Each strain,  $e$ , is expected to couple with the magnetic order parameter,  $m$ , as  $\lambda e m^2$ , where  $\lambda$  is a coupling coefficient, which leads to the expectation:  $e_1 \propto e_2 \propto e_3 \propto V_s \propto m^2$ . Fig. 5a gives the temperature dependences of the individual strains and Fig. 5b,c,d demonstrate internal consistency between them. Obvious breaks in slope at 300 K are most likely to have been an artefact arising from a switch between instruments and the use of different heating rates for the original collection of diffraction data. An additional break in slope is evident in the evolution of  $e_2$ ,  $e_3$  and  $V_s$  at  $\sim 180$  K. Fig. 6 shows the individual strains plotted as  $-e_1$ ,  $-e_2$ ,  $e_3$  and  $-V_s$  (left axis) along with the temperature dependence of  $Q_B^2$  (right axis) where  $Q_B$  is the magnetic order parameter calculated from the Brillouin function for the case of  $J = 1/2$  and  $T_C = 500$  K.

In summary, the spontaneous strains have magnitudes of up to  $\pm \sim 0.002$ , which is comparable with the values of  $e_1$  associated with antiferromagnetic ordering in hematite [37]. The strength of magnetoelastic coupling associated with the ordering transitions at high temperature is thus comparable for both the  $\epsilon$ - and  $\alpha$ -phases of Fe<sub>2</sub>O<sub>3</sub>. In  $\epsilon$ -Fe<sub>2</sub>O<sub>3</sub> the coupling is strongly anisotropic in a manner that is close to uniaxial, i.e. elongation along the crystallographic  $c$ -direction with more or less uniform contraction in the  $ab$ -plane. The largest contraction occurs along the  $a$ -direction, i.e. the magnetic easy axis along which the magnetic moments order. The data can be described quite well by the evolution of the Brillouin order parameter for  $J = 1/2$  down to  $\sim 300$  K ( $e_1 \propto e_2 \propto e_3 \propto V_s \propto Q_B^2$ ). It shows that the strain variations conform to the pattern expected for a second order transition at  $T_C = \sim 500$  K. There are slight tails in the data up to  $\sim 600$  K, consistent with some precursor ordering. Finally, there is no obvious break in slope of any of the strains at  $\sim 100$ – $150$  K, where the second magnetic transition occurs.

## 4. Results

### 4.1. RUS above room temperature, zero field

Fig. 7 contains data for  $f^2$  and  $Q^{-1}$  from a selection of resonance peaks in spectra collected from four different samples over different temperature intervals between room temperature and  $\sim 925$  K. In each figure the left axis is  $f^2$ , with arbitrary scaling factors applied to values

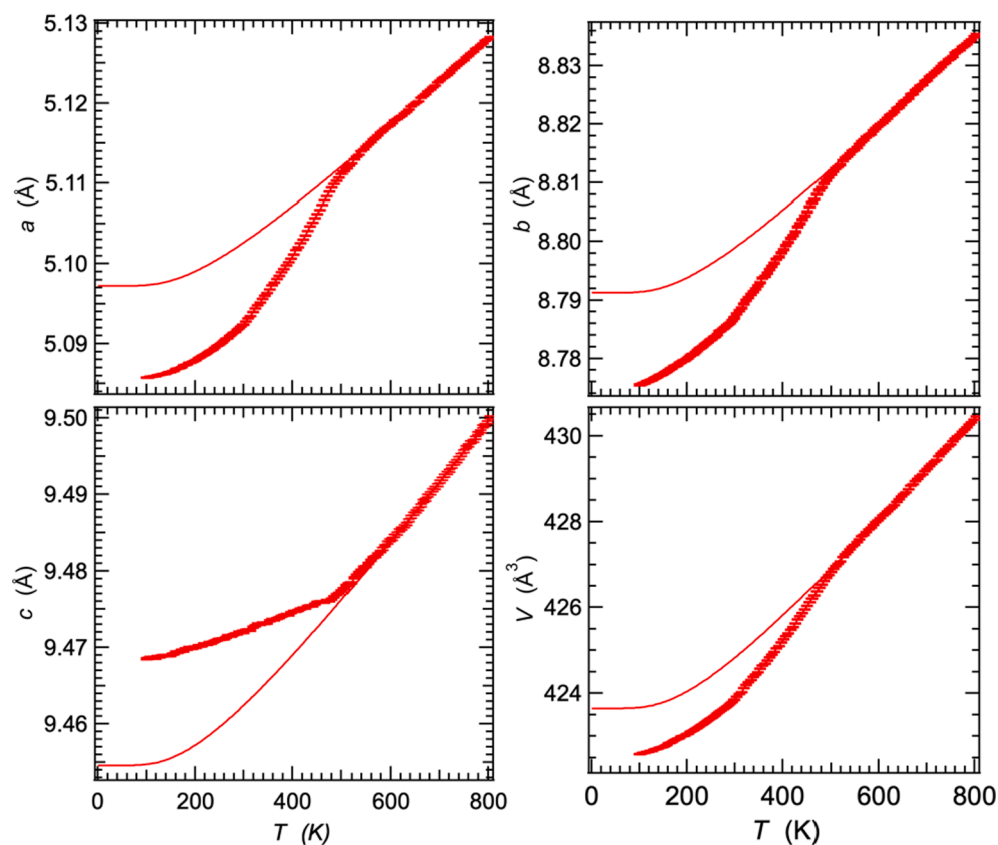


**Fig. 4.** Temperature dependence of the lattice parameters and unit cell volume obtained from synchrotron X-ray powder diffraction of an  $\epsilon$ -Fe<sub>2</sub>O<sub>3</sub> sample with average grain size of 25 nm. The solid curves are baselines obtained by fitting the coth function,  $a_0 = a_1 + a_2 \Theta_s \coth(\Theta_s/T)$ , to data between 598 and 803 K, with the value of  $\Theta_s$  fixed at 300 K. Allowing  $\Theta_s$  to vary freely in the fitting process resulted in different values for each lattice parameter, but the choice of 300 K does not have much influence on the variations of individual strain parameters above room temperature.

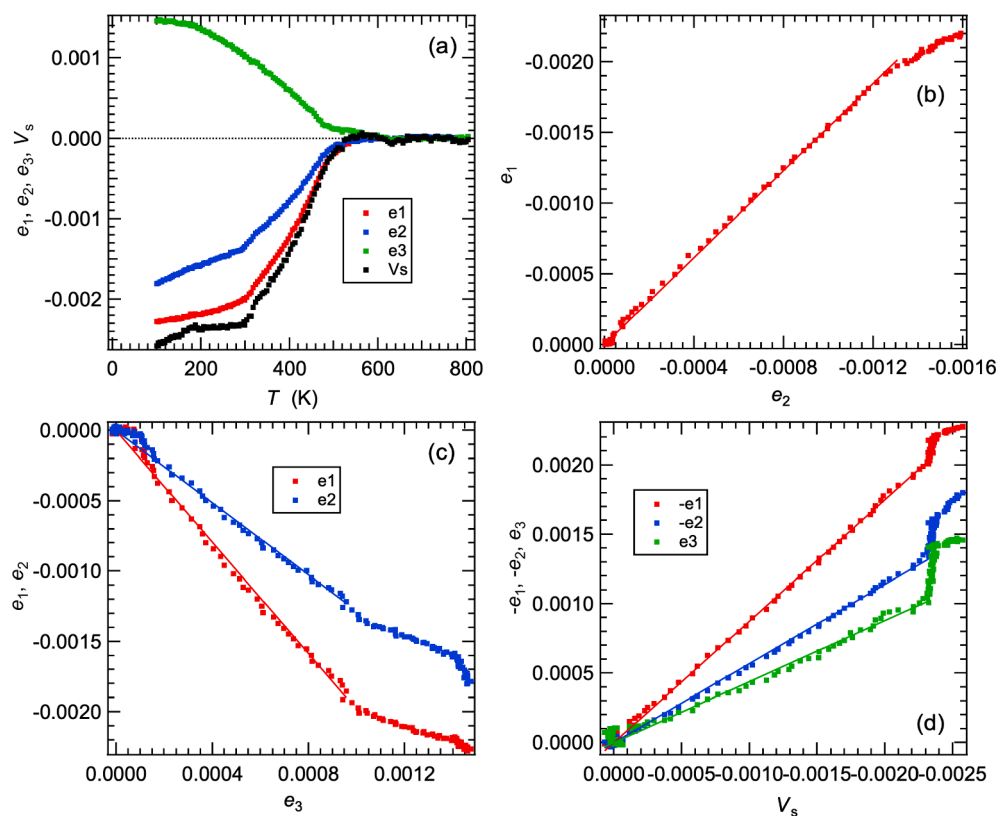


**Fig. 5.** Variations of spontaneous strains determined from the lattice parameter data shown in Fig. 4. (a) Each strain shows a smooth, non-linear decrease between 300 K and the transition temperature of  $\sim$ 500 K, with a tail extending to slightly higher temperatures. (b,c,d) Straight lines passing through the origin in the temperature interval  $\sim$ 300–500 K for strains plotted against each other reveal internal consistency in relation to the expectation that each scales with the square of the driving order parameter for the transition ( $e_1 \propto e_2 \propto e_3 \propto V_s \propto m^2$ ). Deviations from this correlation occur below room temperature.

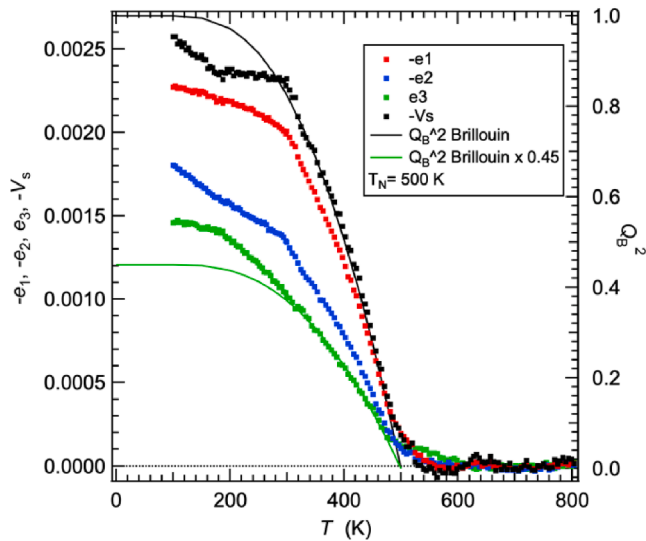


**Fig. 6.** Variations of individual strains, in comparison with variations of  $Q_B^2$  from the Brillouin function with  $J = 1/2$  and  $T_C = 500$  K (black and green curves, right axis). The green curve represents values of  $Q_B^2$  from the Brillouin function multiplied by a scaling factor of 0.45 to match the variation of  $e_3$  above 300 K. There are very obvious breaks in slope at 300 K and more subtle breaks in slope at  $\sim 180$  K.

for individual resonances in order to allow easy comparison of their patterns of evolution.  $Q^{-1}$  variations are shown on the right axis. Sample #5 was subjected to two heating/cooling cycles up to  $\sim 520$  K (Fig. 7a). Sample #2 was subjected to two heating/cooling cycles up to  $\sim 615$  K (Fig. 7b). Sample #3 was first heated to  $\sim 825$  K for  $\sim 45$  min before cycling up to  $\sim 535$  K (Fig. 7c) and then up to  $\sim 925$  K (Fig. 7d). The Second Slice was subjected to one heating/cooling cycle up to  $\sim 535$  K (Fig. 7e). The dimensions and mass were checked at the end of RUS data collection. No overt changes to the shape and density of the samples resulted from cycling up to  $\sim 615$  K, but sample #3 showed a reduction in linear dimensions of  $\sim 0.7\%$  and a reduction in mass of  $\sim 5\%$  after the heating/cooling cycle up to  $\sim 925$  K.

There was a distinct hysteresis in the evolution of  $f^2$  values during the first heating/cooling cycle to temperatures above 500 K. Samples #5 and #2 showed an initial slight stiffening (increasing  $f^2$ ) during heating up to  $\sim 350$  K, followed by slight softening up to  $\sim 450$  K, a relatively steep increase in stiffness up to  $\sim 470$  K, and slight stiffening up to at least  $\sim 520$  K (Fig. 7a, b). Monotonic stiffening with a shallow slope occurred during subsequent cooling down to  $\sim 325$  K, followed by slight softening back to room temperature. Maximum differences in  $f^2$  values between the trajectories of heating and cooling were  $\sim 10\%$ . Relatively steep changes in  $f^2$  between  $\sim 460$  and  $\sim 480$  K during heating of the Second Slice involved softening rather than stiffening and the maximum irreversible change amounted to  $\sim 5\%$  (Fig. 7e). Variations in  $Q^{-1}$  were less marked and involved a decrease with increasing temperature from room temperature to  $\sim 350$  K, particularly in the first cycle, and an increase with increasing temperature above  $\sim 550$  K. The data for Samples #5 and #2 suggest that  $Q^{-1}$  values obtained from spectra collected during the first heating sequence were higher in the temperature interval up to  $\sim 500$  K than in any sequences after they have been exposed to high temperatures.

Clear hysteresis observed in the first heating/cooling cycle of Samples #2 and #5 was not repeated in any of the second cycles.  $f^2$  variations in the second cycle of Sample #5 to  $\sim 520$  K were fully reversible in  $f^2$  and essentially featureless apart from softening with falling temperature below  $\sim 320$  K. The same more-or-less featureless pattern was observed in the second cycle of Sample #2 up to  $\sim 615$  K, but with a small irreversible increase in stiffness seen during cooling (Fig. 7b).

Prior heating to  $\sim 825$  K for a short period led to a nearly reversible evolution in  $f^2$  values, similar to the second cycles of the other samples, though with a slight hysteresis in the softening pattern below  $\sim 350$  K (Fig. 7c). The second cycle of Sample #3 up to  $\sim 925$  K showed a much larger hysteresis, with stiffening by up to  $\sim 12\%$ . There was a change in shape and density of the sample following this heat treatment, however, indicating that at least part of the variation in elastic properties was due to changes to the ceramic such as porosity, grain size or cracking.

The most significant observation in relation to the unusual pattern of hysteretic and non-hysteretic patterns of elastic softening and stiffening shown in Fig. 7 is the absence of a discrete anomaly associated specifically with the expected transition temperature of  $\sim 500$  K. The only hint of a step-like anomaly was a small displacement in resonance frequencies between  $\sim 510$  and  $\sim 500$  K during cooling of the Second Slice. Normal expectations would be that coupling between the order parameter and strain of the form  $\lambda em^2$  at a second order transition would lead to a stepwise softening of individual moduli immediately below the transition point. The characteristic pattern from such a relaxation has been observed for the elastic moduli below the paramagnetic - antiferromagnetic transition at 39 K in  $\text{CoF}_2$ , for example [43]. Such softening requires that the magnetic order parameter can relax on the RUS time-scale of  $\sim 10^{-6}$  s in response to an induced strain. When the relaxation is relatively slow, the expectation is that stiffening or softening in proportion to  $m^2$  would occur below the transition point as a consequence of coupling with the next high order form,  $\lambda e^2 m^2$ . An example of such behaviour is provided by the paramagnetic - antiferromagnetic transition at  $\sim 75$  K in  $\text{YMnO}_3$  at [44].

Evidence of slow relaxation dynamics at room temperature was also obtained unexpectedly during preparation of the rectangular parallelepipeds. The original sintered ceramic was glued to a glass slide using Crystalbond 509, a plastic which requires heating of the sample, the Crystalbond and glass to  $\sim 100^\circ\text{C}$ . Any Crystalbond remaining on the sample was washed off with acetone. It was found that significant short term changes in resonance frequencies were observed before and after drying at  $65^\circ\text{C}$ , following the wash in acetone. In the case of Sample #3, the initial frequency of the lowest frequency resonance before washing in acetone was 439.1 kHz. Fig. 8 shows the variation of  $f^2$  for the same resonance as a function of  $\ln(\text{time})$  from 2 min to  $\sim 24$  hr after removal from the drying oven. The short term effect of the heat treatment was an increase in stiffness by  $\sim 10\%$ , but this reduced almost back to the original value in less than 2 hr. Similarly, the value of  $f^2$  for the same resonance measured after the sample had been heated to  $\sim 825$  K for  $\sim 45$  min was  $2.27 \times 10^5 \text{ kHz}^2$  but became  $2.42 \times 10^5 \text{ kHz}^2$  when measured the following day, corresponding to an increase in shear modulus of  $\sim 7\%$ . It is unlikely that changes in porosity or grain size occurred at or close to room temperature but viscous changes in magnetic domain structure associated with locally preferred orientations of the moments of monodomain crystals could have been possible on this time scale.

#### 4.2. Elastic properties before and after RUS data collection at high temperatures

Attempts to find fits for values of elastic moduli with low rms errors using resonance frequencies at room temperature were not successful. A fit to the frequencies of 20 resonance peaks from Sample #5 before subjecting it to heating/cooling cycles gave isotropic values of  $K$  (bulk modulus) =  $21.6 \pm 0.5$ ,  $G$  (shear modulus) =  $14.60 \pm 0.07$  GPa, with an rms error of 1.5%. Using five independent moduli reduced the rms error to 0.9%:  $C_{11} = 38.6 \pm 2.1$ ,  $C_{33} = 33.8 \pm 0.2$ ,  $C_{12} = 8.8 \pm 0.4$ ,  $C_{13} = -0.12 \pm 0.01$ ,  $C_{44} = 14.59 \pm 0.02$ ,  $(C_{11} - C_{12})/2 = C_{66} = 14.91 \pm 0.06$  GPa. The Voigt-Reuss-Hill average values of  $K$  and  $G$  from these are 14.1 and 15.5 GPa, respectively, providing a more realistic estimate of the bulk modulus. Using nine moduli improved the fit again but probably not in any meaningful way. After cycling to  $\sim 520$  K, an isotropic fit using 24 resonance frequencies gave  $K = 21.6 \pm 0.5$ ,  $G = 14.60 \pm 0.07$  (rms error = 1.2%). The results for five moduli from fitting to 16 resonance

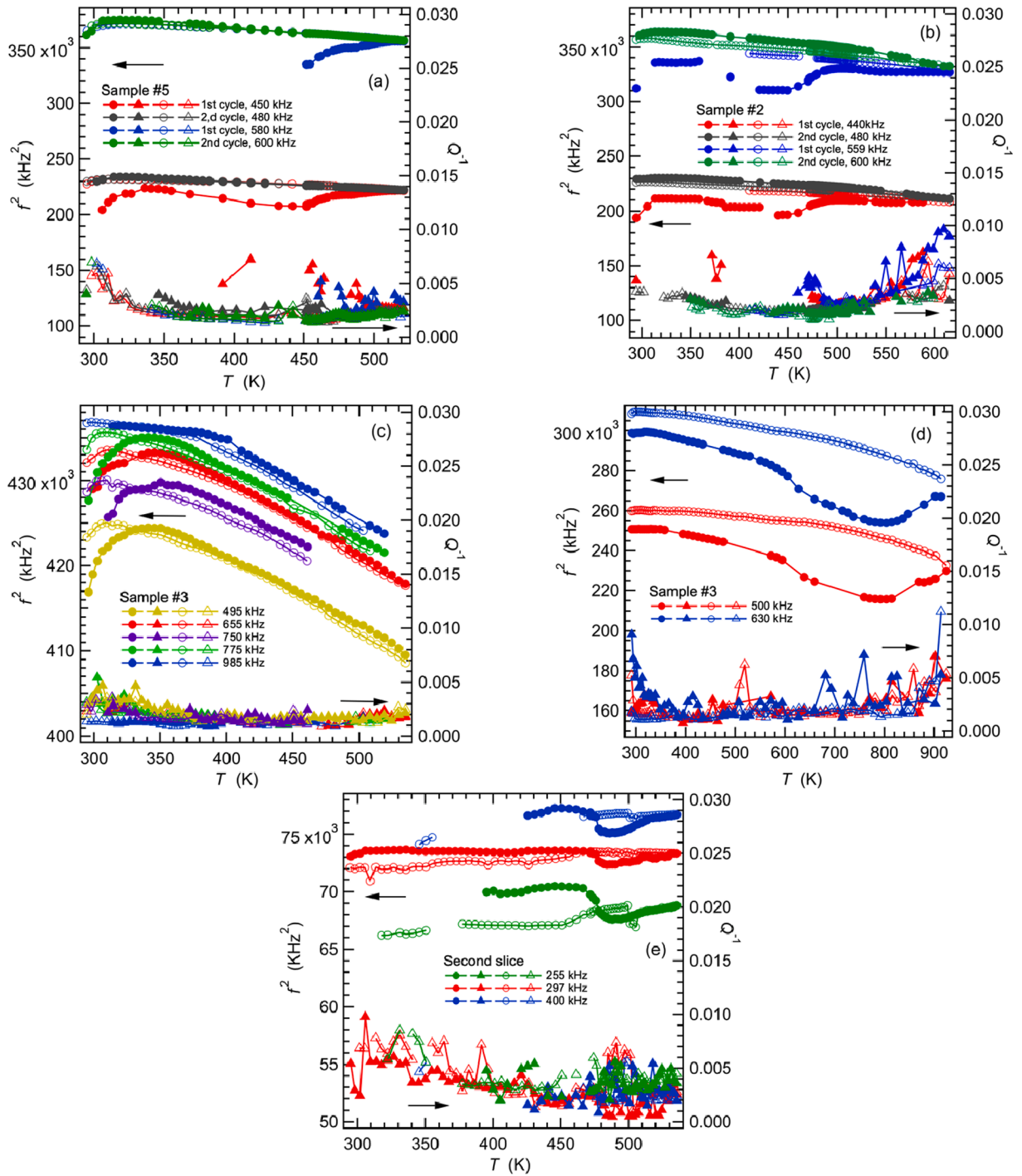


**Fig. 7.**  $f^2$  and  $Q^{-1}$  variations from individual resonances in spectra collected during heating and cooling to high temperatures. Filled symbols = heating, open symbols = cooling. In each graph, values of  $f^2$  for individual resonances have been multiplied by arbitrary scaling factors so that they end up close to each other on the y-axis. Values of frequency given in the captions indicate the approximate frequency of the resonance at room temperature. (a) Sample #5. Two cycles to  $\sim 520$  K.  $f^2$  variations varied irreversibly between heating and cooling in the first cycle and reversibly in the second cycle. (b) Sample #2. Two cycles to  $\sim 615$  K. In this case there was a small shift to higher frequencies between heating and cooling in the second cycle. (c) Sample #3. First heating/cooling cycle to  $\sim 355$  K, after  $\sim 45$  min at  $\sim 830$  K. The evolution of  $f^2$  values was nearly reversible for most of the temperature interval, apart from below  $\sim 350$  K where the trend of softening with falling temperature became established. (d) Sample #3. Second cycle, to  $\sim 925$  K. Irreversible changes in  $f^2$  were accompanied by changes in dimension and mass of the sample. (e) Second Slice. One heating/cooling cycle up to  $\sim 535$  K. In this case the relatively steep changes in  $f^2$  values between  $\sim 460$  and  $\sim 480$  K during heating involved softening rather than stiffening.

frequencies were:  $C_{11} = 45.7 \pm 1.8$ ,  $C_{33} = 44.1 \pm 0.7$ ,  $C_{12} = 9.2 \pm 0.4$ ,  $C_{13} = -8.0 \pm 1.0$ ,  $C_{44} = 17.32 \pm 0.01$ ,  $(C_{11} - C_{12})/2 = C_{66} = 18.25 \pm 0.04$  GPa, with an rms error of 0.4%. The Voigt-Reuss-Hill average values of  $K$  and  $G$  from these are 13.3 and 19.6 GPa, respectively. An rms value of

$\sim 1\%$  indicates a fit that is not robust, and only 16 peaks were used for 5 moduli in the last case. Nevertheless, the general pattern is of some elastic anisotropy for the ceramic and an increase in apparent shear modulus following heat treatment above 500 K.

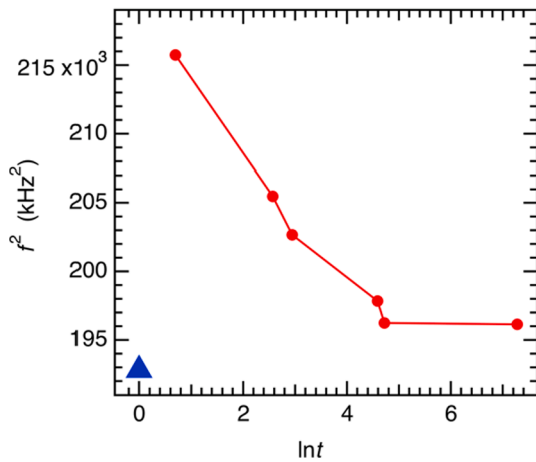


**Fig. 8.** Sample #3. Variation of  $f^2$  for a resonance peak with frequency near 440 kHz, as a function of  $\ln t$ , where  $t$  is time in minutes at room temperature following  $\sim 1$  hr at  $\sim 65$  °C. The blue triangle placed at  $\ln t = 0$  is the value of  $f^2$  before the sample was washed in acetone and placed in the drying oven.

Values of  $Q^{-1}$  measured from peak widths in spectra collected at room temperature with the sample sitting directly on the piezoelectric transducers were  $\sim 0.011$  and  $\sim 0.012$  before and after cycling to  $\sim 520$  K for Sample #5. Values for Sample #3 before heating and 24 hr after heating at  $\sim 825$  K were 0.014 and 0.007. Absolute values shown in Fig. 7 are different from these due to the fact the signal had to pass along alumina buffer rods in the high temperature instrument.

#### 4.3. RUS below room temperature in zero field

Fig. 9 shows the variations of  $f^2$  and  $Q^{-1}$  from fitting of a representative peak with frequency near 480 kHz in primary RUS spectra collected from Sample #1. The spectra were collected in 5 K steps through the temperature interval 5–295 K. Overall,  $f^2$  values increased smoothly and had progressively shallower slope with falling temperature, as expected for the normal variation of elastic moduli as  $T \rightarrow 0$  K. There is a slight stiffening trend below  $\sim 50$  K but there are no discrete anomalies between 80 and 150 K which would correlate with the known phase transition in this interval. Moreover, there are no anomalies that might correlate with the change in the evolution of spontaneous strains at  $\sim 180$  K.  $Q^{-1}$  values reduced with falling temperature, though with the suggestion of a broad peak centred at  $\sim 140$  K and of a stronger peak

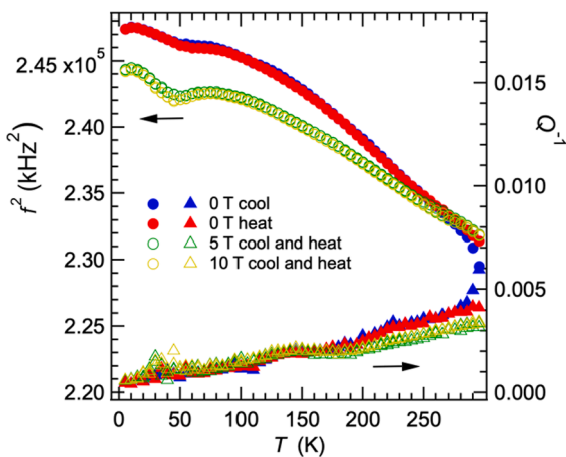


**Fig. 9.** Sample #1. Evolution of  $f^2$  and  $Q^{-1}$  obtained from fitting a resonance peak with frequency near 480 kHz at room temperature during cooling and heating in 5 K steps between 295 and 5 K.

centred at  $\sim 35$  K. These patterns of evolution for the peak near 480 kHz were corroborated by essentially the same variations of  $f^2$  and  $Q^{-1}$  obtained from fitting of a resonance peak with frequency near 800 kHz. In both sets of data there is a slight hysteresis between heating and cooling for  $f^2$  values in the intervals  $\sim 50$ – $80$  and  $\sim 250$ – $295$  K.

Details of the stiffening at low temperatures in zero field were investigated in a separate cooling/heating sequence between 80 and 20 K with collection of spectra at intervals of 0.5 K. Variations of  $f^2$  and  $Q^{-1}$  for a representative resonance peak with frequency near 1135 kHz show a break in slope between  $\sim 60$  and  $\sim 65$  K, distinct hysteresis between heating and cooling of  $f^2$  values and a selection of peaks in  $Q^{-1}$  (Fig. 10). At these temperatures, the values of  $Q^{-1}$  are close to 0.001 and the peaks in  $Q^{-1}$  increase above the baseline by only up to  $\sim 0.0004$ , which is close to the overall limit of reproducibility. There is some uncertainty as to their exact form, therefore, but the superficial appearance is of stiffening, consistent with Debye-like relaxation/freezing below  $\sim 65$  K of a succession of point defects or components of a microstructure which were weakly coupled with strain. Differences between heating and cooling in the temperature interval  $\sim 20$ – $65$  K (Fig. 10) and at higher temperatures (Fig. 9) could then have been due to irreversible changes in the local configurations of magnetic moments of individual grains that depend on thermal history when the sample as a whole is unpoled. This interpretation is consistent with the result discussed below, and also shown in Fig. 9, that the hysteresis of  $f^2$  values between heating and cooling disappears in a field of 5 or 10 T when the ceramic is magnetically poled.

The observation of irreversible changes in both  $f^2$  and  $Q^{-1}$  in zero field prompted a more systematic investigation of the time dependence of elastic properties at low temperatures. First the sample was allowed to reach thermal equilibrium at 200 K. It was then cooled to a set point between 25 and 150 K and spectra collected as a function of time. Cooling rates between 200 K and each set point were  $\sim 0.3$ – $0.4$  K.min $^{-1}$ . Fig. 11a shows the direction of change observed at each temperature and Fig. 11b shows the change in observed  $f^2$  values,  $\Delta f^2$ , between the first and subsequent measured frequencies for the resonance peak near 815 kHz. At 100, 125 and 150 K, equilibration to constant values of  $\Delta f^2$  occurred within  $\sim 8$  h of reaching the set point. Values of  $\Delta f^2$  were smaller at 75 K, and essentially zero at 25 K. The direction of change at 50 K was the reverse of that seen at higher temperatures, with no indication that a constant value had been reached even after  $\sim 3$  days.

Curves shown in Fig. 11b are fits to the data using a stretched exponential function:

$$\Delta f^2(t) = f_{\infty}^2 - (f_{\infty}^2 - f_0^2) \exp\left(-\left(\frac{t}{\tau}\right)^{\beta}\right), \quad (1)$$

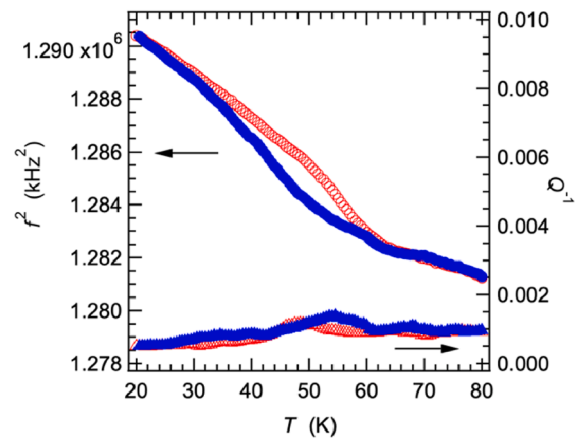


**Fig. 10.** Sample #1. Variations of  $f^2$  and  $Q^{-1}$  for a resonance peak with frequency near 1135 kHz, collected during cooling (blue filled symbols) followed by heating (red, open symbols) in steps of 0.5 K between 80 and 20 K.

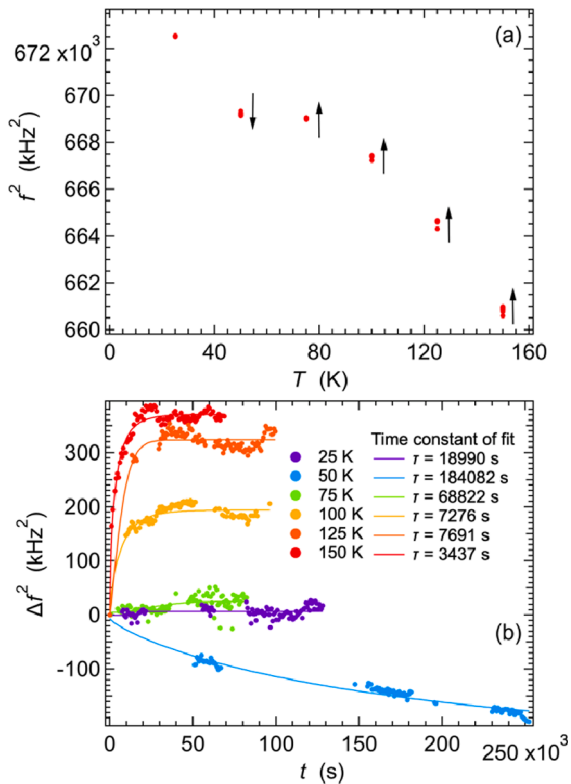


**Fig. 11.** Sample #1. Time-dependent measurements at different fixed temperatures for a resonance near 815 kHz after rapid cooling from 200 K. (a) Variations of  $f^2$  at each set temperature; arrows indicate the direction of change as a function of time. (b)  $\Delta f^2$  is the change in  $f^2$  after time  $t$  with respect to the value obtained from the first measurement at each temperature. Curves through the data are fits of Equation (1) with  $\beta = 0.8$ . Values of the time constant,  $\tau$ , from the fits shown for each temperature are listed in the inset.

where  $f_\infty^2$  is the value of  $f^2$  that the peak would eventually relax to,  $f_0^2$  is the value obtained from the first measurement and  $\tau$  is the relaxation time constant. Fit values for the exponent,  $\beta$ , varied between 0.6 and 1.5. Constraining the value of  $\beta$  to 1 provided an adequate description of the data at most temperatures but a value of  $\sim 0.8$ , as used for the curves shown in Fig. 11b, was necessary to also give a good fit to the 50 K data. An Arrhenius plot of the time constants for 75–150 K yielded an apparent activation energy of  $40 \pm 10$  meV.

#### 4.4. RUS below room temperature: Variable temperature with constant applied field of 5 or 10 T

Measurements with variable temperature at constant field were started by increasing the field to 5 or 10 T when the sample was at room temperature. Variations of  $f^2$  and  $Q^{-1}$  from the 480 kHz resonance peak in spectra collected during cooling and heating in each of these fields are compared with the zero field data in Fig. 9. There are no major differences in the overall patterns but, in detail,  $f^2$  values at 5 and 10 T were very slightly higher than in zero field between 295 and  $\sim 270$  K, indistinguishable at  $\sim 270$  K and then progressively lower with falling temperature below 270 K. The maximum degree of softening due to application of the field was  $\sim 2\%$ . Changes in trend below  $\sim 65$  K in zero field became a distinct minimum centred at  $\sim 50$  K, with a steeper recovery below this, when the field was 5 or 10 T. The magnitude of the dip in  $f^2$  centred at  $\sim 50$  K was very slightly greater in 10 T than 5 T fields. Measurements at 5 K all revealed a small final softening.

$Q^{-1}$  values were lower than in zero field at temperatures between 295 and  $\sim 180$  K but, below this, indistinguishable from values in the applied field. The combined data appear to confirm the presence of the

broad peak in  $Q^{-1}$  centred at  $\sim 140$  K and the more pronounced loss peak centred at  $\sim 35$  K.

According to Fig. 2c, the sample would have been fully poled at 5 T. There are almost no differences between  $f^2$  data collected at 5 and 10 T (Fig. 9), implying that the main effect of the field on elastic properties, in comparison with zero field, was due to poling. Changes in the elastic moduli due to the conventional effects of magnetostriction thus appear to have been negligible, at least between 5 and 10 T. The disappearance of differences in  $f^2$  values between heating and cooling in high fields is consistent with the hysteresis seen in zero field also being associated with changes in magnetic domain structure.

#### 4.5. RUS below room temperature: Variable field at constant temperature

In order to investigate the nature of possible relaxation/freezing processes in the vicinity of 60 K, spectra were collected with changing field up to 10 T at 295 K and 50 K. Variations of  $f^2$  and  $Q^{-1}$  from a resonance peak with frequency near 152 kHz at room temperature are

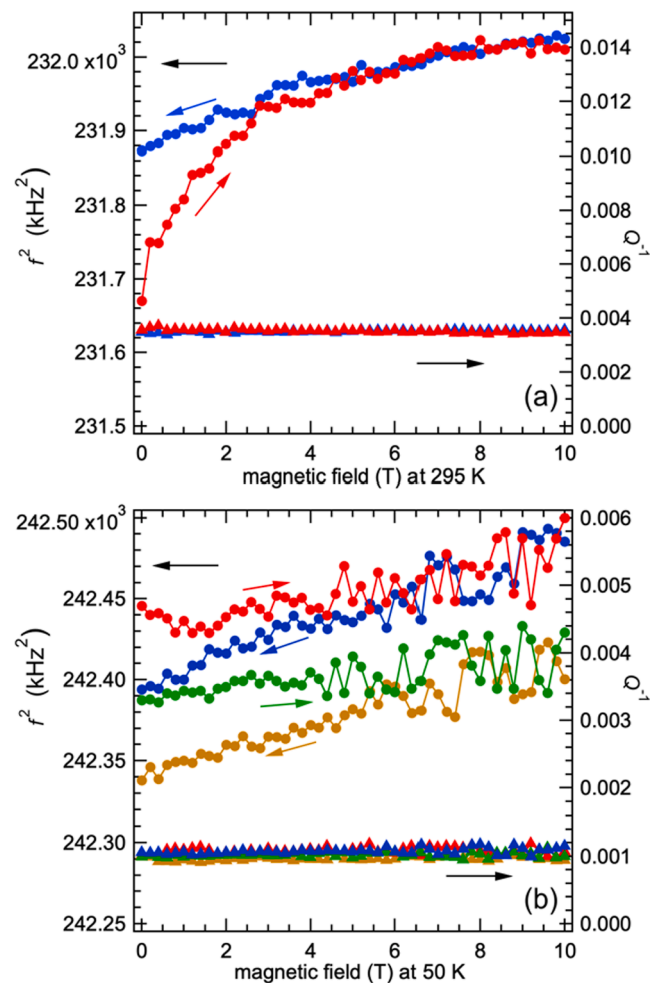


**Fig. 12.** Variations of  $f^2$  and  $Q^{-1}$  as a function of field at constant temperature from a resonance peak with frequency near 480 kHz at room temperature. (a) 295 K: There is a marked hysteresis in  $f^2$  values below  $\sim 2$  T between magnetisation (red) and demagnetisation (blue).  $Q^{-1}$  values barely changed throughout the full cycle. 2 T is approximately the coercive field at 300 K. (b) 50 K: Red markers show the first magnetisation, blue the first demagnetisation (cycle 1), green the second magnetisation and brown the second demagnetisation (cycle 2). A steady drift to lower values of  $f^2$  through the full sequence is superimposed on a weak trend of increasing values with increasing field. The dominant feature of  $Q^{-1}$  variations is a barely resolved drift to lower values with time through the two cycles.

shown in Fig. 12. The evolution of  $f^2$  at 295 K (Fig. 12a) can be easily understood through reference to the  $M-H$  loop shown for 300 K in Fig. 2c. Progressive poling by alignment of initially randomly oriented moments of individual grains, or of a domain structure with local alignment of moments, was accompanied by stiffening from  $f^2 \approx 231.7 \text{ kHz}^2$  to  $\sim 231.9 \text{ kHz}^2$  at  $\sim 2.5 \text{ T}$ , by which stage the sample would have been fully poled. Beyond that,  $f^2$  increased with shallower slope as a function of increasing field and decreased reversibly to the same value with reducing field.  $f^2$  values of the poled sample diverged from those of the unpoled sample as the field reduced back to zero and the difference between the two in zero field corresponds to a difference in shear modulus of  $\sim 0.07\%$ .  $Q^{-1}$  values barely changed throughout the full cycle, implying that any contribution from motion of magnetic domain walls to the acoustic loss under dynamic stress must have been small or zero.

$f^2$  values also increased with increasing field and decreased with decreasing field at 50 K, but the overall pattern was quite different in character (Fig. 12b). In the first cycle, the trend was reversible at fields above  $\sim 5 \text{ T}$ , by which point the sample must have been fully poled (based on the  $M-H$  loops shown in Fig. 2c). Divergence with reducing field below  $\sim 5 \text{ T}$  could have been due simply to a difference in shear modulus between unpoled and poled ceramics, amounting to  $\sim 0.02\%$  in zero field. However, the irreversible evolution continued through the second cycle and there was clearly an additional long term, time-dependent drift of progressive elastic softening. There was no particular trend of  $Q^{-1}$  values with changing field, other than a barely resolved drift to slightly lower values throughout the two cycles.

## 5. Discussion

### 5.1. Structure and properties of the ceramic

Preparation of a ceramic sample with the same grain size and magnetic properties as the nanocrystalline powder used for the starting material has allowed the magnetoelastic behaviour of  $\epsilon\text{-Fe}_2\text{O}_3$  to be investigated through the temperature interval  $\sim 2\text{--}925 \text{ K}$ , including the three expected magnetic phase transitions at  $\sim 110$ ,  $\sim 500 \text{ K}$  and  $\sim 850 \text{ K}$ . Some contributions to the overall acoustic loss must have arisen from porosity and/or grain boundary effects but, in the first instance, these would be expected to provide a background that was either constant or smoothly increasing with temperature. Variations in  $Q^{-1}$  due to properties of the sintered crystals themselves should be identifiable as irregularities superimposed on this background. Some proportion of irreversible variations in the effective shear modulus during the heating/cooling cycle to  $\sim 925 \text{ K}$  must have been due to changes of grain size, changes of porosity or conversion to  $\alpha\text{-Fe}_2\text{O}_3$  but, if the irreversible variations in elastic properties during the first cycle of Sample #5 to  $\sim 520 \text{ K}$  had been due to such changes, some additional changes would have been expected during the second cycle - and none were observed (Fig. 7a). There was a small increase in  $f^2$  during the second cycle of Sample #2 to  $620 \text{ K}$  (Fig. 7b), suggesting that initiation of irreversible changes relating to grain size, porosity, or proportions of phases, as mentioned above, requires heating to at least  $\sim 550 \text{ K}$  for times of hours.

A previous result from consideration of the dynamic response of non-interacting grains of  $\epsilon\text{-Fe}_2\text{O}_3$  in a pulsed magnetic field [45] is that surface effects are of minor importance for the magnetic behaviour of grains with dimensions of 25–100 nm but are significant for grains with dimensions of less than 10 nm. Given the grain size range shown in Fig. 1b, it is probably safe to assume that the observed magnetic and elastic properties reported here from spectra collected without cycling to temperatures above  $\sim 550 \text{ K}$  represent bulk properties of  $\epsilon\text{-Fe}_2\text{O}_3$  in porous ceramic form. Evidence that the ceramic had some texturing due to the uniaxial stress applied during sintering, such as from pore distributions or grain orientations, is provided both by differences in magnetisation between three orthogonal directions (Fig. 3b,c) and by the elastic anisotropy found in attempts to fit five moduli to resonance

frequencies measured at room temperature. Elastic anisotropy due to texturing would have persisted throughout the RUS measurements.

The crystallographic space group of  $\epsilon\text{-Fe}_2\text{O}_3$  at room temperature is  $Pna2_1$ . This polar space group could, in principle, develop as a consequence of a ferroelectric phase transition from a non-polar parent structure with space group  $Pbcn$  [46]. However, although ferroelectric switching appears to be possible in thin films [46] it has not been observed in bulk samples at temperatures down to  $10 \text{ K}$  [11]. This does not rule out the possibility that crystals are piezoelectric, as allowed by their crystallographic space group symmetry. In addition, direct evidence of piezomagnetism is provided by the magnetic polarisation of the bulk ceramic samples in the direction of the stress applied during sintering (Fig. 3a). The magnetic space group at room temperature is  $Pna'2_1'$  [no. 33.147] [12] and a paramagnetic parent structure would have magnetic space group  $Pna2_1'$  [33.145], which is permitted to be piezomagnetic.

With respect to elastic properties, the parent and product structures of purely ferroelectric or magnetic transitions would both be orthorhombic and it follows that poling of magnetic or ferroelectric domains in the lower symmetry structure would not result in a change in the number of independent components of the elastic modulus tensor. Net values of the piezomagnetic and piezoelectric coefficients for a polycrystalline sample with random orientations of both crystallographic axes and magnetic moments should be zero but magnetic poling (even with the crystallographic axes remaining randomly oriented) should result in finite values of the effective coefficients of a bulk sample. As has been shown in the case of piezoelectric moduli [47] and suggested for piezomagnetic moduli in the case of  $\text{YMnO}_3$  [44] and  $\text{ErMnO}_3$  [48], resonance frequencies in an RUS experiment depend on both the elastic and piezo moduli. In other words, changes in preferred alignments of magnetic moments of individual grains should result in changes in measured values of  $f^2$  due to changes in the effective piezomagnetic and/or piezoelectric moduli of the bulk sample. This effect is proposed here as an explanation of most of the observed variations in  $f^2$  values. Any changes in elastic properties arising from the more conventional consequences of coupling between the magnetic order parameter and strain appear to be small.

The magnetic domain structure of the sintered ceramic disc is not known, but the magnetisation data in Fig. 3a show that rectangular parallelepipeds cut from it inherited a degree of polarisation which developed during cooling under stress from the sintering temperature of  $\sim 623 \text{ K}$ . There are two limiting magnetic states to consider, bearing in mind that each crystal was expected to be monodomain: random distributions of moments for every individual grain, and maximal poling of moments and local domain states in which there is a degree of correlation of the orientations of moments of individual grains over a finite length scale. These would be characterised by maximum differences in acoustic resonance frequencies arising from the contributions of piezo moduli. If there is any imbalance in the net moment due to an imbalance of domain states or the domains have large enough dimensions, variations in magnitude between the limiting resonance frequencies would be expected. Values of  $f^2$  measured as a function of temperature at 5 and 10 T (Fig. 10) should then represent those of a maximally poled sample. The hysteretic changes in  $f^2$  values observed as a function of increasing and decreasing magnetic field at 295 K (Fig. 12a) are also attributed to changes in piezo moduli of the bulk samples arising from poling.

An emerging focus for future work on the functional properties of ceramic  $\epsilon\text{-Fe}_2\text{O}_3$  is clearly on the nature of magnetic domains encompassing multiple grains which themselves are monodomain. In this context, simulations of magnetic interactions between nanocrystals using theoretical approaches analogous to those used by Knizek et al [49] for simulations of interaction parameters at an atomic scale would be instructive.

## 5.2. High temperature behaviour

Variations of the spontaneous strains shown in Fig. 6 are consistent with the view that the magnetic/structural changes can be understood in terms of a co-elastic, thermodynamically continuous transition between two orthorhombic structures with a transition temperature of  $\sim 500$  K and a tail of short range order up to  $\sim 550$  K. The strains vary up to  $\pm \sim 0.002$  and scale with the square of the driving order parameter through coupling terms of the form  $\lambda e m^2$ , as in the case of the paramagnetic  $\rightarrow$  canted antiferromagnetic transition at  $\sim 955$  K in  $\alpha$ -Fe<sub>2</sub>O<sub>3</sub> [37]. This coupling would, in turn, be expected to give discontinuous and reversible softening of the elastic moduli below the transition point with the form typical for co-elastic transitions, such as has been observed for the shear modulus at the paramagnetic-antiferromagnetic transition in CoF<sub>2</sub> [43]. No consistent anomaly associated with the expected transition point during heating or cooling of any of the samples has been found, however, implying both that the relaxation time of the order parameter in response to an induced strain is longer than  $\sim 10^{-6}$  s and that coupling of the form  $\lambda e^2 m^2$  in  $\epsilon$ -Fe<sub>2</sub>O<sub>3</sub> is weak.

Instead of the expected pattern of elastic anomalies due to strain/order parameter coupling at a second order transition, irreversible stiffening of the parallelepipeds and softening of the Second Slice occurred during heating between  $\sim 450$  and  $480$  K. If these irreversible variations had been due to densification of the ceramic and/or conversion to  $\alpha$ -Fe<sub>2</sub>O<sub>3</sub>, all the samples should have shown the same changes, whereas the Second Slice showed softening instead of stiffening. Hysteretic effects in the close vicinity of phase transitions are generally due to first order character, but the spontaneous strain data provide no evidence that the magnetic transition at  $\sim 500$  K could be first order. Over wider temperature intervals below the transition point, differences in properties between heating and cooling are typically due to changes in microstructure. Focus is therefore on the evolution of magnetic domains.

Changes to the domain structure of individual parallelepipeds inherited from the sintered disc would have been subject to kinetic constraints on the motion of domain walls and flipping of the moments of individual grains at room temperature. Based on the attribution of changes in elastic properties being determined primarily by changes in effective piezomagnetic and/or piezoelectric moduli of the bulk sample, reorganisation of the domain structure to some more nearly equilibrium configuration for a rectangular parallelepiped only became possible when it was heated to temperatures above  $\sim 450$  K. On cooling from above the transition point, the evidence of both magnetisation (Fig. 3a) and  $f^2$  variations (Fig. 7) is that a new domain structure developed with a net moment of zero for the sample as a whole.

Other measurements on samples in which  $\epsilon$ -Fe<sub>2</sub>O<sub>3</sub> grains were suspended in silica also show changes near  $450$ – $480$  K which can be interpreted in terms of kinetic effects. These include a bifurcation at  $\sim 480$  K between magnetisation measured under field cooled and zero field cooled conditions, using a field of  $1$  kOe [12,13], and a frequency dependent peak in the real part of ac susceptibility at  $\sim 467$  K ( $30$  Hz) or  $\sim 470$  K ( $1$  kHz) [12]. Both observations are consistent with the view that, with falling temperature below a transition point of  $\sim 500$  K in zero field, the moments of individual grains remain mobile to some degree but become frozen in below  $\sim 470$  K. The real component of ac susceptibility has a maximum when  $\omega\tau (=2\pi f\tau) = 1$ , where  $\omega$  is the angular frequency,  $\tau$  is the relaxation time and  $f$  is the measuring frequency. The relaxation time, presumably for domain wall motion, is  $\sim 5 \times 10^{-3}$  s at  $\sim 467$  K and  $\sim 2 \times 10^{-4}$  s at  $\sim 470$  K. This temperature dependence coincides with a steep decrease in coercive field with increasing temperature, becoming close to zero at  $\sim 475$  K [12].

$Q^{-1}$  values showed an irreversible evolution through the transition point, with values  $\sim 0.005$  reducing to  $\sim 0.002$  during subsequent cooling, as measured with the sample held between buffer rods in the high temperature instrument (Fig. 7a,b). Similarly,  $Q^{-1}$  values from Sample #3 reduced from  $0.014$  to  $0.007$  due to annealing at  $\sim 825$  K, as measured on a room temperature system with the sample sitting directly

between the transducers. The change in loss is presumably related to the change in domain structure, though magnetic domain walls in  $\epsilon$ -Fe<sub>2</sub>O<sub>3</sub> are not ferroelastic and therefore would not necessarily be expected to move in response to an applied stress.

The RUS data do not exhibit signatures of the phase transition at  $\sim 850$  K unveiled by Garcia-Muñoz et al [12]. There is an increase in  $f^2$  values during heating above  $\sim 825$  K but no anomaly in the data collected during subsequent cooling (Fig. 7d) and at least some of the observed stiffening is most likely related to the change in mass and dimensions of the sample.

## 5.3. Behaviour near room temperature

Magnetic hysteresis loops for  $\epsilon$ -Fe<sub>2</sub>O<sub>3</sub> provide evidence for changes in magnetic properties close to room temperature. They typically show a kink at zero magnetic field at  $300$  K, as shown here also at  $200$  K in Fig. 2b. Kohout et al [16] ascribed this to the presence of  $\gamma$ -Fe<sub>2</sub>O<sub>3</sub> as an impurity phase but Ma et al [17] ruled this possibility out on the basis that the same anomaly was observed in a sample with known, low impurity content. The same kink was reported at  $260$  K by Tseng et al [19]. Fig. 2 of Ohkoshi et al [8] shows, however, that the magnitude of the kink is a function of grain size and that it is absent from hysteresis loops measured at room temperature for grains with diameters of  $\sim 24$  nm. The effect clearly arises from a steep decline in coercive field with reducing grain size to  $\sim 0$  for grains with diameters less than  $\sim 6$  nm [8,50]. From the perspective of magnetism, therefore, samples of  $\epsilon$ -Fe<sub>2</sub>O<sub>3</sub> with a spread of grain sizes can only be regarded as heterogeneous.

A survey of the literature has not revealed any specific anomalies in magnetic or structure properties to correlate with the hysteretic and time-dependent elastic softening below  $\sim 350$  K displayed in Figs. 7 and 8, respectively. In the absence of any correlation with other properties, this softening is tentatively interpreted as being due to changes in piezo moduli arising from changes in domain structures which, perhaps, were related to the lower coercive field of grains belonging to the finer size range of the variation shown in Fig. 1b.

## 5.4. Low temperature behaviour

The quality of resonance signals in primary RUS spectra at low temperatures was certainly adequate to confirm that there were no overt elastic or anelastic anomalies associated with a transition in the temperature interval  $\sim 85$ – $150$  K (Fig. 9). Diffraction data of Gich et al [5,6] indicate that the high and low temperature structures coexist over much of this interval, which would result in smoothing out of any discrete elastic anomalies. A wide two phase field could also account for the broad, weak peak in  $Q^{-1}$  if the loss mechanism involves motion of interfaces between the two phases. These results are understandable if there is only very slight strain contrast between the two structures, as is consistent also with the absence of any discrete anomalies in spontaneous strains between  $150$  and  $100$  K (Fig. 2). Tseng et al [19] identified subtle variations in ratios of unit cell dimensions at a level of up to  $\sim 10^{-4}$  between  $\sim 80$  and  $150$  K, signifying that the total contrast in strains is not necessarily zero, however.

As noted above, differences in  $f^2$  values between zero and  $5/10$  T fields can be understood as being due to changing contributions of piezoelectric/piezomagnetic moduli for ceramic samples which start off with multidomain microstructures and become poled at fields above  $\sim 3$  T. The effect of poling seems also to have resulted in fully reversible evolution of  $f^2$  between heating and cooling (Fig. 9), consistent with the view that hysteretic effects in zero field are due primarily to changes in magnetic domain configurations. The magnitude of differences between zero field and  $5/10$  T increases with falling temperature and does not appear to be influenced by the transition to the incommensurate structure. No overt evidence has been found for any metamagnetic transitions either in the data obtained with varying temperature at constant field or

with varying field at constant temperature.

Individual strain variations (Fig. 6) display a break in slope at  $\sim 180$  K which correlates with the onset of the substantial reduction in coercivity originally reported by Gich et al [15] and Sakurai et al [14]. In addition, values of  $Q^{-1}$  were higher when measured in zero field than when measured in a field of 5 or 10 T above  $\sim 180$  K but the same below  $\sim 180$  K. The correlation between elimination of magnetic domain walls in the poled sample and a lowering of acoustic loss suggests that the walls themselves might be the main contributors to the loss mechanism in the temperature interval  $\sim 180$ – $300$  K even though they are not ferroelastic and would not necessarily be expected to move in response to an applied shear stress.

The absence of any difference in loss behaviour between zero field and 5/10 T at temperatures below  $\sim 180$  K suggests a change in properties related to the steep reduction in coercive field ahead of the transition to the incommensurate phase. As a matter of pure speculation, this is reminiscent of a transition that occurs by cation ordering in the silicate mineral solid solution, plagioclase feldspar ( $\text{NaAlSi}_3\text{O}_8$ - $\text{CaAl}_2\text{Si}_2\text{O}_8$ ), in which the principal driving force for a commensurate to incommensurate transition appears to be stabilisation of antiphase boundaries. The antiphase boundaries are defects with a positive excess energy at some temperatures and compositions but then become stable features of the incommensurate structure [51,52]. On this basis, the steep reduction in coercivity seen for  $\epsilon$ - $\text{Fe}_2\text{O}_3$  would be an equivalent indication that the excess energy of magnetic domain changes from positive to negative below  $\sim 180$  K and that they end up contributing to the stability of the incommensurate structure below  $\sim 110$  K.

The main feature of the evolution of elastic properties at the lowest temperatures is the break in slope of  $f^2$  at  $\sim 65$  K, as shown in detail for zero field in Fig. 10. Other properties which display changes at similar temperatures are, firstly, a minimum in the ratio of remnant magnetisation to saturation magnetisation at  $\sim 60$ – $80$  K [15] and, secondly, an anomaly in the real part of the dielectric susceptibility, which is independent of frequency (up to the THz range) and displays thermal hysteresis (a dielectric peak at 75 K is more distinct when measured on heating) [11]. The latter relates to the dynamics of some microstructure or defects. Glassy behaviour is suggested by the fact that an equilibrium state, with respect to elastic properties, is not achieved after prolonged times at 50 K (Fig. 11b, 12b). In the absence of any more definitive information, it is concluded only that the RUS results show freezing of some aspect of the structure or microstructure which is coupled with strain. The question remains as to whether this relates to a distribution of the moments of individual grains with the incommensurate structure or freezing of some other type of magnetoelastic defect.

Absent from the RUS data is any evidence of strain coupling with the dynamic effects responsible for the frequency dependent peak in dielectric loss between  $\sim 100$  K at 10 Hz and  $\sim 180$  K at 300 kHz that was reported by Kadlec et al [11]. This dielectric anomaly falls in almost the same temperature and frequency range as variations of capacitance and conductance seen by Gich et al [6], and was attributed to electronic excitations.

### 5.5. Evolution of order parameter(s)

The analysis of spontaneous strains presented in Fig. 6 fits with a conventional description of a magnetic transition at 500 K and a temperature dependence of the order parameter down to  $\sim 300$  K according to the Brillouin function with  $J = 1/2$ . If there is an additional magnetic transition at  $\sim 850$  K where the change in magnetic space group  $Pna2_11'$  -  $Pna'2_1'$  actually occurs, the transition at  $\sim 500$  K would be isosymmetric,  $Pna'2_1' - Pna'2_1'$ . In general, isosymmetric transitions are expected to be first order in character [53], which does not fit with all the evidence for continuity of structural and magnetic properties at  $\sim 500$  K. If there is only one high temperature transition where symmetry is broken, an alternative view is that there are two order parameters with the same symmetry and bilinear coupling between them

[54]. Both order parameters would have non zero values below the transition point at  $\sim 850$  K. They would follow different temperature dependences and have a crossover at  $\sim 500$  K between intervals where one varies more strongly than the other. Garcia-Muñoz et al [12] reported that magnetic ordering above  $\sim 500$  K involves only two of the  $\text{Fe}^{3+}$  sublattices while all four contribute to the ordering below this.

There is no evidence in the RUS data for a transition at  $\sim 850$  K but the same arguments in relation to the dynamics and magnitude of strain/order parameter coupling as used to explain the absence of an anomaly at  $\sim 500$  K still apply. Alternative measurements, such as of heat capacity and of elastic properties using lower dynamic frequencies, would be needed to resolve the issue of whether the behaviour at  $\sim 500$  K is a discrete phase transition or a crossover for two discrete order parameter with the same symmetry but different temperature dependences.

## 6. Conclusions

$\epsilon$ - $\text{Fe}_2\text{O}_3$  continues to challenge conventional descriptions of magnetic phase transitions in comparison with the well-established properties and behaviour of other polymorphs of  $\text{Fe}_2\text{O}_3$ . Changes in elastic and anelastic properties measured at frequencies in the vicinity of  $\sim 1$  MHz do not conform to the patterns of softening or stiffening that would be expected at a classical phase transition in which spontaneous strains couple with the square of the order parameter. The absence of elastic anomalies at  $\sim 500$  K indicates that the relaxation times for changes in the magnetic order parameter in response to an induced strain are slower than  $\sim 10^{-5}$ - $10^{-6}$  s. Unusual and hysteretic changes in elastic properties are, instead, attributed to bulk piezomagnetic/piezoelectric properties arising from the configuration of magnetic domains created by interactions between grains which are themselves monodomain. There is no evidence for any significant strain contrast between the commensurate and incommensurate structures at the low temperature transition but there is evidence of freezing of some aspect of microstructure or other defects in the stability field of the incommensurate structure, below  $\sim 65$  K.

The ceramic form of  $\epsilon$ - $\text{Fe}_2\text{O}_3$  produced by Spark Plasma Sintering has magnetic, piezoelectric and/or piezomagnetic properties which can be tuned by choice of grain size and thermomagnetic history. It has high coercivity at room temperature, requiring fields of a few Teslas to reorient the net moment acquired parallel to the direction of applied stress during sintering. The orientation of magnetisation can, alternatively, be manipulated in fields as low as 50 Oe by cooling to below  $\sim 100$  K, where the coercivity becomes low. An interesting question remains as to whether these magnetic properties can also be manipulated with an electric field.

### CRedit authorship contribution statement

**C.R.S. Haines:** Investigation, Formal analysis, Writing – review & editing. **M. Gich:** Funding acquisition, Investigation, Validation, Writing – review & editing. **J.L. García-Muñoz:** Investigation, Formal analysis, Writing – review & editing. **A. Romaguera:** Investigation, Formal analysis. **Z. Ma:** Investigation, Formal analysis. **M.B. Costa:** Investigation. **M.A. Carpenter:** Funding acquisition, Conceptualization, Formal analysis, Writing – original draft, Writing – review & editing.

### Declaration of Competing Interest

The authors declare the following financial interests/personal relationships which may be considered as potential competing interests: M.A.Carpenter reports financial support was provided by Leverhulme Trust. M.A.Carpenter reports financial support was provided by Natural Environment Research Council. M.A.Carpenter reports financial support was provided by Engineering and Physical Sciences Research Council. M.Gich reports financial support was provided by the Spanish Ministry

of Science, Innovation, and Universities. M.Gich reports financial support was provided by European Regional Development Fund. M.Gich reports financial support was provided by FUNFUTURE. M.Gich reports financial support was provided by European Research Council. M.B. Costa reports financial support was provided by European Union Horizon 2020.

## Data availability

Data will be made available on request.

## Acknowledgements

This work was funded by grant no. RPG-2016-298 from the Leverhulme Trust. RUS facilities in Cambridge were established through grants from the Natural Environment Research Council (Grants No. NE/B505738/1 and No. NE/F017081/1) and the Engineering and Physical Sciences Research Council (Grant No. EP/I036079/1) to MAC. We also acknowledge financial support from the Spanish Ministry of Science, Innovation, and Universities (Grants No. RTI2018-098537-B-C21, cofunded by ERDF from EU, and FUNFUTURE (CEX2019-000917-S)) and funding from the European Research Council (ERC) under the European Union's Horizon 2020 research and innovation programme (grant agreement No. 819623). ALBA synchrotron is also acknowledged. Support is acknowledged from the European Union Horizon 2020 Research and Innovation Programme under Marie Skłodowska-Curie grant 861046 (BIOREMIA) for MBC.

## References

- H. Xu, S. Lee, H. Xu, Luogufengite: A new nano-mineral of Fe<sub>2</sub>O<sub>3</sub> polymorph with giant coercive field, *Am. Mineral.* 102 (2017) 711–719, <https://doi.org/10.2138/am-2017-5849>.
- S. Lee, H. Xu, Size-dependent phase map and phase transformation kinetics for nanometric iron(III) oxides ( $\gamma \rightarrow \epsilon \rightarrow \alpha$  Pathway), *J. Phys. Chem. C* 120 (2016) 13316–13322, <https://doi.org/10.1021/acs.jpcc.6b05287>.
- J.A. Sans, V. Monteselegro, G. Garbarino, M. Gich, V. Cerantola, V. Cuartero, M. Monte, T. Iriñe, A. Muñoz, C. Popescu, Stability and nature of the volume collapse of  $\epsilon$ -Fe<sub>2</sub>O<sub>3</sub> under extreme conditions, *Nat. Commun.* 9 (2018) 4554, <https://doi.org/10.1038/s41467-018-06966-9>.
- E. Tronc, C. Chaneac, J.P. Jolivet, Structural and magnetic characterization of epsilon-Fe<sub>2</sub>O<sub>3</sub>, *J. Solid State Chem.* 139 (1998) 93–104, <https://doi.org/10.1006/jssc.1998.7817>.
- M. Gich, C. Frontera, A. Roig, E. Taboada, E. Molins, H.R. Rechenberg, J. D. Ardisson, W.A.A. Macedo, C. Ritter, V. Hardy, J. Sort, V. Skumryev, J. Nogués, High- and low-temperature crystal and magnetic structures of epsilon-Fe<sub>2</sub>O<sub>3</sub> and their correlation to its magnetic properties, *Chem. Mater.* 18 (2006) 3889–3897, <https://doi.org/10.1021/cm060993l>.
- M. Gich, C. Frontera, A. Roig, J. Fontcuberta, E. Molins, N. Bellido, C. Simon, C. Fleta, Magnetolectric coupling in epsilon-Fe<sub>2</sub>O<sub>3</sub> nanoparticles, *Nanotechnology* 17 (2006) 687–691, <https://doi.org/10.1088/0957-4484/17/3/012>.
- J. Tuček, R. Zbořil, A. Namai, S. Ohkoshi,  $\epsilon$ -Fe<sub>2</sub>O<sub>3</sub>: An advanced nanomaterial exhibiting giant coercive field, millimeter-wave ferromagnetic resonance, and magnetolectric coupling, *Chem. Mater.* 22 (2010) 6483–6505, <https://doi.org/10.1021/cm101967h>.
- S. Ohkoshi, A. Namai, K. Imoto, M. Yoshikiyo, W. Tarora, K. Nakagawa, M. Komine, Y. Miyamoto, T. Nasu, S. Oka, H. Tokoro, Nanometer-size hard magnetic ferrite exhibiting high optical-transparency and nonlinear optical-magnetolectric effect, *Sci. Rep.* 5 (2015) 14414, <https://doi.org/10.1038/srep14414>.
- K. Xu, J.S. Feng, Z.P. Liu, H.J. Xiang, Origin of ferrimagnetism and ferroelectricity in room-temperature multiferroic  $\epsilon$ -Fe<sub>2</sub>O<sub>3</sub>, *Phys. Rev. Applied* 9 (2018), 044011, <https://doi.org/10.1103/PhysRevApplied.9.044011>.
- M. Gich, I. Fina, A. Morelli, F. Sánchez, M. Alexe, J. Gázquez, J. Fontcuberta, A. Roig, Multiferroic iron oxide thin films at room temperature, *Adv. Mater.* 26 (2014) 4645–4652, <https://doi.org/10.1002/adma.201400990>.
- C. Kadlec, F. Kadlec, V. Goian, M. Gich, M. Kempa, S. Rols, M. Savinov, J. Prokleska, M. Orlita, S. Kam, Electromagnon in ferrimagnetic  $\epsilon$ -Fe<sub>2</sub>O<sub>3</sub> nanograin ceramics, *Phys. Rev. B* 88 (2013), 104301, <https://doi.org/10.1103/PhysRevB.88.104301>.
- J.L. García-Muñoz, A. Romaguera, F. Fauth, J. Nogués, M. Gich, Unveiling a new high-temperature ordered magnetic phase in  $\epsilon$ -Fe<sub>2</sub>O<sub>3</sub>, *Chem. Mater.* 29 (2017) 9705–9713, <https://doi.org/10.1021/acs.chemmater.7b03417>.
- M. Kurmoo, J.-L. Rehspringer, A. Hutlova, C. D'Orléans, S. Vilminot, C. Estournès, D. Niznansky, Formation of Nanoparticles of  $\epsilon$ -Fe<sub>2</sub>O<sub>3</sub> from yttrium iron garnet in a silica matrix: an unusually hard magnet with a Morin-like transition below 150 K, *Chem. Mater.* 17 (2005) 1106–1114, <https://doi.org/10.1021/cm0482838>.
- S. Sakurai, J. Jin, K. Hashimoto, S. Ohkoshi, Reorientation phenomenon in a magnetic phase of  $\epsilon$ -Fe<sub>2</sub>O<sub>3</sub> nanocrystal, *J. Phys. Soc. Jpn.* 74 (2005) 1946–1949, <https://doi.org/10.1143/jpsj.74.1946>.
- M. Gich, A. Roig, C. Frontera, E. Molins, J. Sort, M. Popovici, G. Chouteau, D.M. Y. Marero, J. Nogués, Large coercivity and low-temperature magnetic reorientation in epsilon-Fe<sub>2</sub>O<sub>3</sub> nanoparticles, *J. Appl. Phys.* 98 (2005), 044307, <https://doi.org/10.1063/1.1997297>.
- J. Kohout, P. Brázda, K. Závěta, D. Kubániová, T. Kmječ, L. Kubíčková, M. Klementová, E. Šantavá, A. Lančok, The magnetic transition in  $\epsilon$ -Fe<sub>2</sub>O<sub>3</sub> nanoparticles: Magnetic properties and hyperfine interactions from Mössbauer spectroscopy, *J. Appl. Phys.* 117 (2015) 17D505, <https://doi.org/10.1063/1.4907610>.
- Z. Ma, A. Romaguera, F. Fauth, J. Herrero-Martín, J.L. García-Muñoz, M. Gich, Magnetic properties of Cr-substituted  $\epsilon$ -(Fe<sub>1-x</sub>Cr<sub>x</sub>)<sub>2</sub>O<sub>3</sub> nanoparticles with epsilon structure, *J. Magn. Magn. Mat.* 506 (2020), 166764, <https://doi.org/10.1016/j.jmmm.2020.166764>.
- M. Gich, C. Frontera, A. Roig, E. Taboada, E. Molins, H.R. Rechenberg, J. D. Ardisson, W.A.A. Macedo, C. Ritter, V. Hardy, J. Sort, V. Skumryev, J. Nogués, High- and low-temperature crystal and magnetic structures of  $\epsilon$ -Fe<sub>2</sub>O<sub>3</sub> and their correlation to its magnetic properties, *Chem. Mater.* 18 (2006) 3889–3897, <https://doi.org/10.1021/cm060993l>.
- Y.C. Tseng, N.M. Souza-Neto, D. Haske, M. Gich, C. Frontera, A. Roig, M. van Veenendaal, J. Nogués, Nonzero orbital moment in high coercivity epsilon-Fe<sub>2</sub>O<sub>3</sub> and low-temperature collapse of the magnetocrystalline anisotropy, *Phys. Rev. B* 79 (2009), 094404, <https://doi.org/10.1103/PhysRevB.79.094404>.
- M.A. Carpenter, E.K.H. Salje, A. Graeme-Barber, Spontaneous strain as a determinant of thermodynamic properties for phase transitions in minerals, *Eur. J. Mineral.* 10 (4) (1998) 621–691, <https://doi.org/10.1127/ejm/10/4/0621>.
- W. Rehwald, The study of structural phase transitions by means of ultrasonic experiments, *Adv. Phys.* 22 (1973) 721–755, <https://doi.org/10.1080/00018737300101379>.
- B. Lüthi, W. Rehwald, Ultrasonic studies near structural phase transitions, *Topics in Curr. Phys.* 23 (1981) 131–184, [https://doi.org/10.1007/978-3-642-81531-7\\_4](https://doi.org/10.1007/978-3-642-81531-7_4).
- M.A. Carpenter, E.K.H. Salje, Elastic anomalies in minerals due to structural phase transitions, *Eur. J. Mineral.* 10 (4) (1998) 693–812, <https://doi.org/10.1127/ejm/10/4/0693>.
- M. Gich, A. Roig, E. Taboada, E. Molins, C. Bonafos, E. Snoeck, Stabilization of metastable phases in spatially restricted fields: the case of the Fe<sub>2</sub>O<sub>3</sub> polymorphs, *Faraday Discuss.* 136 (2007) 345–354, <https://doi.org/10.1039/B616097B>.
- M.A. Schneider, W.S. Rasband, K.W. Eliceiri, NIH Image to ImageJ: 25 years of image analysis, *Nat. Methods* 9 (2012) 671–675, <https://doi.org/10.1038/nmeth.2089>.
- L. Lutterotti, P. Scardi, P. Maistrelli, LSI - a computer program for simultaneous refinement of material structure and microstructure, *J. Appl. Crystallogr.* 25 (1992) 459–462, <https://doi.org/10.1107/S0021889892001122>.
- T. Bublath, D. Goll, Temperature dependence of the magnetic properties of L1<sub>0</sub>-FePt nanostructures and films, *J. Appl. Phys.* 108 (2010) 113910, <https://doi.org/10.1063/1.3512906>.
- J.M.D. Coey, *Magnetism and Magnetic Materials*, Cambridge University Press, Cambridge, 2010, <https://doi.org/10.1017/CBO9780511845000>.
- Ö. Özdemir, D.J. Dunlop, T.S. Berquó, Morin transition in hematite: Size dependence and thermal hysteresis, *Geochem. Geophys. Geosyst.* 9 (10) (2008), Q10201, <https://doi.org/10.1029/2008GC002110>.
- J. Schiemer, L.J. Spalek, S.S. Saxena, C. Panagopoulos, T. Katsufuji, A. Bussmann-Holder, J. Köhler, M.A. Carpenter, Magnetic field and in situ stress dependence of elastic behavior in EuTiO<sub>3</sub> from resonant ultrasound spectroscopy, *Phys. Rev. B* 93 (2016), 054108, <https://doi.org/10.1103/PhysRevB.93.054108>.
- D.M. Evans, J.A. Schiemer, M. Schmidt, H. Wilhelm, M.A. Carpenter, Defect dynamics and strain coupling to magnetization in the cubic helimagnet Cu<sub>2</sub>OSeO<sub>3</sub>, *Phys. Rev. B* 95 (2017), 094426, <https://doi.org/10.1103/PhysRevB.95.094426>.
- R.E.A. McKnight, M.A. Carpenter, T.W. Darling, A. Buckley, P.A. Taylor, Acoustic dissipation associated with phase transitions in lawsonite, CaAl<sub>2</sub>Si<sub>2</sub>O<sub>7</sub>(OH)<sub>2</sub>·H<sub>2</sub>O, *Am. Mineral.* 92 (2007) 1665–1672, <https://doi.org/10.2138/am.2007.2568>.
- R.E.A. McKnight, T. Moxon, A. Buckley, P.A. Taylor, T.W. Darling, M.A. Carpenter, Grain size dependence of elastic anomalies accompanying the  $\alpha$ - $\beta$  phase transition in polycrystalline quartz, *J. Phys.: Condens. Matter* 20 (7) (2008) 075229, <https://doi.org/10.1088/0953-8984/20/7/075229>.
- M.A. Carpenter, A. Buckley, P.A. Taylor, T.W. Darling, Elastic relaxations associated with the Pm-3m - R-3c transition in LaAlO<sub>3</sub>: III. Superattenuation of acoustic resonances, *J. Phys.: Condens. Matter* 22 (2010), 035405, <https://doi.org/10.1088/0953-8984/22/3/035405>.
- A. Migliori, J.L. Sarrao, W.M. Visscher, T.M. Bell, M. Lei, Z. Fisk, R.G. Leisure, Resonant ultrasound spectroscopic techniques for measurement of the elastic moduli of solids, *Physica B: Condensed Matter* 183 (1–2) (1993) 1–24, [https://doi.org/10.1016/0921-4526\(93\)90048-B](https://doi.org/10.1016/0921-4526(93)90048-B).
- N.B. Nešković, B. Babić, J. Konstantinović, High temperature anomalous behaviour of the crystal lattice of hematite, *Phys. Stat. Sol.* 41 (1977) K133–K136, <https://doi.org/10.1002/pssa.2210410252>.
- L. Oravova, Z. Zhang, N. Church, R.J. Harrison, C.J. Howard, M.A. Carpenter, Elastic and anelastic relaxations accompanying magnetic ordering and spin-flop transitions in hematite, Fe<sub>2</sub>O<sub>3</sub>, *J. Phys.: Condens. Matter* 25 (11) (2013) 116006, <https://doi.org/10.1088/0953-8984/25/11/116006>.
- H.-W. Meyer, M.A. Carpenter, A. Graeme-Barber, P. Sondergeld, W. Schranz, Local and macroscopic order parameter variations associated with low temperature phase transitions in lawsonite, CaAl<sub>2</sub>Si<sub>2</sub>O<sub>7</sub>(OH)<sub>2</sub>·H<sub>2</sub>O, *Eur. J. Mineral.* 12 (6) (2000) 1139–1150, <https://doi.org/10.1127/0935-1221/2000/0012-1139>.

- [39] H.-W. Meyer, S. Marion, P. Sondergeld, M.A. Carpenter, K.S. Knight, S.A. T. Redfern, M.T. Dove, Displacive components of the low-temperature phase transitions in lawsonite, *Am. Mineral.* 86 (2001) 566–577, <https://doi.org/10.2138/am-2001-0419>.
- [40] P. Sondergeld, W. Schranz, A.V. Kityk, M.A. Carpenter, E. Libowitzky, Ordering behaviour of the mineral lawsonite, *Phase Trans.* 71 (2000) 189–203, <https://doi.org/10.1080/01411590008229651>.
- [41] M.A. Carpenter, H.-W. Meyer, P. Sondergeld, S. Marion, K.S. Knight, Spontaneous strain variations through the low temperature phase transitions of deuterated lawsonite, *Am. Mineral.* 88 (2003) 534–546, <https://doi.org/10.2138/am-2003-0407>.
- [42] E.K.H. Salje, B. Wruck, H. Thomas, Order-parameter saturation and low-temperature extension of Landau theory, *Z. Phys. B* 82 (1991) 399–404, <https://doi.org/10.1007/BF01357186>.
- [43] R.I. Thomson, T. Chatterji, M.A. Carpenter, CoF<sub>2</sub>: a model system for magnetoelastic coupling and elastic softening mechanisms associated with paramagnetic ↔ antiferromagnetic phase transitions, *J. Phys.: Condens. Matter* 26 (14) (2014) 146001, <https://doi.org/10.1088/0953-8984/26/14/146001>.
- [44] R.I. Thomson, T. Chatterji, C.J. Howard, T.T.M. Palstra, M.A. Carpenter, Elastic anomalies associated with structural and magnetic phase transitions in single crystal hexagonal YMnO<sub>3</sub>, *J. Phys.: Condens. Matter* 26 (4) (2014) 045901, <https://doi.org/10.1088/0953-8984/26/4/045901>.
- [45] D.A. Balaev, I.S. Poperechny, A.A. Krasikov, K.A. Shaikhutdinov, A.A. Dubrovskiy, S.I. Popkov, A.D. Balaev, S.S. Yakushkin, G.A. Bukhtiyarova, O.N. Martyanov, Y. L. Raikher, Dynamic magnetization of  $\epsilon$ -Fe<sub>2</sub>O<sub>3</sub> in pulse field: Evidence of surface effect, *J. Appl. Phys.* 117 (6) (2015) 063908, <https://doi.org/10.1063/1.4907586>.
- [46] X. Guan, L. Yao, K.Z. Rushchanskii, S. Inkinen, R. Yu, M. Ležaić, F. Sánchez, M. Gich, S. Dijken, Unconventional ferroelectric switching via local domain wall motion in multiferroic  $\epsilon$ -Fe<sub>2</sub>O<sub>3</sub> films, *Adv. Electron. Mater.* 6 (4) (2020), 1901134, <https://doi.org/10.1002/aelm.201901134>.
- [47] J. Schreuer, Elastic and piezoelectric properties of La<sub>3</sub>Ga<sub>5</sub>SiO<sub>14</sub> and La<sub>3</sub>Ga<sub>5.5</sub>Ta<sub>0.5</sub>O<sub>14</sub>: an application of resonant ultrasound spectroscopy, *IEEE Trans. Ultrasonics, Ferroelectrics, Freq. Cont.* 49 (2002) 1474–1479, <https://doi.org/10.1109/tuffc.2002.1049728>.
- [48] C.M. Fernandez-Posada, C.R.S. Haines, D. Evans, Z. Yan, E. Bourret, D. Meier, M. A. Carpenter, Magnetoelastic properties of multiferroic hexagonal ErMnO<sub>3</sub>, *J. Magn. Magn. Mat.* 554 (2022), 169277, <https://doi.org/10.1016/j.jmmm.2022.169277>.
- [49] K. Knížek, P. Novák, Z. Jiráč, Exchange interactions in  $\epsilon$ -Fe<sub>2</sub>O<sub>3</sub>: GGA + U calculations, *J. Phys.: Condens. Matter* 33 (2021), 155502, <https://doi.org/10.1088/1361-648X/abdb13>.
- [50] A.A. Dubrovskiy, D.A. Balaev, K.A. Shaykhutdinov, O.A. Bayukov, O.N. Pletnev, S. S. Yakushkin, G.A. Bukhtiyarova, O.N. Martyanov, Size effects in the magnetic properties of  $\epsilon$ -Fe<sub>2</sub>O<sub>3</sub> nanoparticles, *J. Appl. Phys.* 118 (2015), 213901, <https://doi.org/10.1063/1.4936838>.
- [51] M.A. Carpenter, Mechanisms and kinetics of Al-Si ordering in anorthite: I. Incommensurate structure and domain coarsening, *Am. Mineral.* 76 (1991) 1110–1119.
- [52] M.A. Carpenter, in: *Feldspars and their Reactions*, Springer Netherlands, Dordrecht, 1994, pp. 221–269.
- [53] A.G. Christy, Isosymmetric structural phase transitions: phenomenology and examples, *Acta Cryst. B* 51 (1995) 753–757, <https://doi.org/10.1107/S0108768195001728>.
- [54] E.K.H. Salje, V. Devarajan, Phase transitions in systems with strain-induced coupling between two order parameters, *Phase Trans.* 6 (1986) 235–247, <https://doi.org/10.1080/0141159860821830>.